

A novel higher-order numerical method for parabolic integro-fractional differential equations based on wavelets and $L2-1_\sigma$ scheme

Sudarshan Santra^a, Ratikanta Behera^{a,*}

^a*Department of Computational and Data Sciences, Indian Institute of Science, Bangalore, India.*

Abstract

This study aims to construct an efficient and highly accurate numerical method to solve a class of parabolic integro-fractional differential equations, which is based on wavelets and $L2-1_\sigma$ scheme. Specifically, the Haar wavelet decomposition is used for grid adaptation and efficient computations, while the high order $L2-1_\sigma$ scheme is considered to discretize the time-fractional operator. Second-order discretizations are used to approximate the spatial derivatives to solve the one-dimensional problem, while a repeated quadrature rule based on trapezoidal approximation is employed to discretize the integral operator. In contrast, we use the semi-discretization of the proposed two-dimensional model based on the $L2-1_\sigma$ scheme for the fractional operator and composite trapezoidal approximation for the integral part. The spatial derivatives are then approximated using two-dimensional Haar wavelets. In this study, we investigated theoretically and verified numerically the behavior of the proposed higher-order numerical methods. In particular, stability and convergence analyses are conducted. The obtained results are compared with those of some existing techniques through several graphs and tables, and it is shown that the proposed higher-order methods have better accuracy and produce less error compared to the $L1$ scheme in favor of fractional-order integro-partial differential equations.

Keywords: Integro-partial differential equation, Caputo derivative, Higher-order scheme, Haar wavelet, $L2-1_\sigma$ scheme, Error analysis.

2020 MSC: 45K05, 45D05, 26A33, 65M06.

1. Introduction

During the past few decades, the qualitative analysis of fractional differential equations (FDEs) and fractional-order integro-differential equations (FOIDEs) has gained popularity owing to their practical application in numerous fields of science and technology, including control theory, cryptography, neural networks, options trading, and viscoelasticity. For a detailed study, refer to [1, 2, 3] and the references therein. In the context of FDEs/FOIDEs, the current state of the system depends not only on the current time but also on its past

*Corresponding author

Email addresses: sudarshans@iisc.ac.in (Sudarshan Santra), ratikanta@iisc.ac.in (Ratikanta Behera)

history over a certain time span, which makes the analysis and solution of the problems more interesting. Furthermore, the singular behavior of the solution of a fractional-order system not only differs from the classical integer-order systems but also poses a greater challenge for solving them. For a detailed study of fractional-order problems with initial singularities, we direct the reader's attention to the work by Chen *et al.* [4] and, Santra and Mohapatra [5]. In general, finding an analytical solution to fractional differential equations involving integral operators is impractical, because a lot of iterations are required, which makes the process more time-consuming. So one has to rely on the semi-analytical and numerical methods. A few semi-analytical approaches, such as the Adomian decomposition method [6], homotopy analysis method [7], and variational iteration method [8], can be used to solve FOIDEs. In addition, many equivalent articles are available in the literature on the numerical solutions of FDEs and FOIDEs based on finite difference/element methods [9, 10]. A finite difference solution for an FDE/FOIDE at a particular time level depends on the solutions at all previous time levels; however, this is not the case for integer order differential systems [11, 12]. Furthermore, most of the phenomena exhibit localized high-frequency behavior. This makes the process more complicated; therefore, it is mandatory to develop efficient numerical techniques to tackle fractional-order systems.

Wavelets are numerical concepts that allow one to represent a function in terms of basis functions, and wavelet-based numerical methods take advantage of the fact that functions with localized regions of sharp transitions are well compressed using wavelet decomposition [13, 14]. This property allows local grid refinement up to an arbitrarily small scale without a drastic increase in the number of collocation points; thus, high-resolution computations can be performed only in regions where sharp transitions occur. It is worth mentioning that in the last few decades, the Haar wavelet method has become a valuable tool for solving ODEs and PDEs, as well as integral and integro-differential equations, and many authors have verified it [15, 16]. Specifically, the Haar wavelet is more popular owing to its beneficial properties such as orthogonality, simple applicability, and compact support. It requires less effort and maintains the accuracy of the solution and its derivatives.

The main objective of this study is to develop efficient numerical methods to solve the following class of time-fractional integro-partial differential equations (TFIPDEs):

Problem I: One-dimensional TFIPDEs

$$\left\{ \begin{array}{l} \partial_t^\alpha \mathcal{U}(x, t) - \mathcal{L}\mathcal{U}(x, t) + \mu \int_0^t \mathcal{K}(x, t - \xi) \mathcal{U}(x, \xi) d\xi = f(x, t), \\ (x, t) \in \Omega := (0, L) \times (0, T], \text{ with} \\ \mathcal{U}(x, 0) = g(x) \text{ for } x \in [0, L], \mathcal{U}(0, t) = h_1(t) \text{ and } \mathcal{U}(L, t) = h_2(t) \text{ for } t \in (0, T], \end{array} \right. \quad (1.1)$$

Problem II: Two-dimensional TFIPDEs

$$\begin{cases} \partial_t^\alpha \mathcal{U}(x, y, t) - \mathfrak{L}\mathcal{U}(x, y, t) + \mu \int_0^t \mathcal{K}(x, y, t - \xi) \mathcal{U}(x, y, \xi) d\xi = f(x, y, t), \\ (x, y) \in \mathcal{G} := (0, 1) \times (0, 1), \quad t \in (0, T], \text{ with } \mathcal{U}(x, y, 0) = g(x, y) \text{ for } (x, y) \in \overline{\mathcal{G}}, \\ \mathcal{U}(0, y, t) = h_1(y, t) \text{ and } \mathcal{U}(1, y, t) = h_2(y, t) \text{ for } (y, t) \in [0, 1] \times (0, T], \\ \mathcal{U}(x, 0, t) = h_3(x, t) \text{ and } \mathcal{U}(x, 1, t) = h_4(x, t) \text{ for } (x, t) \in [0, 1] \times (0, T], \end{cases} \quad (1.2)$$

where $\alpha \in (0, 1)$. ∂_t^α denotes the fractional Caputo derivative of order α , defined as [17]: $\partial_t^\alpha \mathcal{U}(\cdot, t) = \mathfrak{J}^{1-\alpha} \mathcal{U}_t(\cdot, t)$ for $t \in (0, T]$, where $\mathfrak{J}^{1-\alpha}$ denotes the Riemann-Liouville fractional integral operator defined as $\mathfrak{J}^{1-\alpha} \mathcal{U}(\cdot, t) = \frac{1}{\Gamma(1-\alpha)} \int_{s=0}^t (t-s)^{-\alpha} \mathcal{U}(\cdot, s) ds$, $t \in (0, T]$. Furthermore, the gradient operators are given by

$$\begin{cases} \mathcal{L}\mathcal{U} := p(x) \mathcal{U}_{xx} - q(x) \mathcal{U}_x - r(x) \mathcal{U}(x, t), \\ \mathfrak{L}\mathcal{U} := p_1(x, y) \mathcal{U}_{xx} + p_2(x, y) \mathcal{U}_{yy} - q_1(x, y) \mathcal{U}_x - q_2(x, y) \mathcal{U}_y - r_1(x, y) \mathcal{U}(x, y, t). \end{cases}$$

Again, $p, q, r, f, g, h_1, h_2, h_3, h_4, p_1, p_2, q_1, q_2$ are sufficiently smooth functions with $r(x) \geq 0$, $p(x) \geq p_0 > 0$ $\forall x \in [0, L]$ and $r_1(x, y) \geq 0$, $p_1(x, y) \geq \tilde{p}_0 > 0$, $p_2(x, y) \geq \hat{p}_0 > 0$ $\forall (x, y) \in \mathcal{G}$. Kernel \mathcal{K} is smooth and considered positive and real-valued. μ is the fixed positive constant. Further, Problem I satisfies the minimal compatibility condition $h_1(0) = g(0)$, $h_2(0) = g(L)$, whereas Problem II satisfies $h_1(y, 0) = g(0, y)$, $h_2(y, 0) = g(1, y)$, $h_3(x, 0) = g(x, 0)$, $h_4(x, 0) = g(x, 1)$, which ensures that the solution lies in $C(\bar{\Omega}, \mathbb{R})$. If $\mu = 0$, then (1.1) and (1.2) become time-fractional subdiffusion problems, which have been extensively studied in the literature [18, 19]; for that problems, it is well known that given smooth and compatible data, nevertheless the solution $\mathcal{U}(\cdot, t)$ will exhibit a weak singularity at the initial time $t = 0$. Despite the presence of such singularities of the temporal derivatives in the solution, many researchers make a priori assumption that higher-order temporal derivatives of the solution are smooth on the closed domain, in order to deal with the numerical analysis of finite difference techniques for solving them using Taylor expansions in their truncation error analyses [20, 21, 22]. Likewise, in this paper, we assume that the solutions of the proposed one and two-dimensional TFIPDEs are sufficiently smooth in order to adapt a highly accurate numerical scheme in the temporal direction. In the following section, we describe a physical motivation for the present research.

1.1. A physical motivation

Consider the problem:

$$\begin{cases} \partial_t^\alpha \mathcal{U}(x, t) - p(x) \mathcal{U}_{xx}(x, t) = f(x, t), \quad (x, t) \in \Omega, \\ \mathcal{U}(x, 0) = g(x) \text{ for } x \in [0, L], \\ \mathcal{U}(0, t) = h_1(t) \text{ and } \mathcal{U}(1, t) = h_2(t) \text{ for } t \in (0, T]. \end{cases} \quad (1.3)$$

Model (1.3) represents a nonhomogeneous fractional-order sub-diffusion model that describes the well-known fractional time random walk [23], which can be obtained from (1.1) by taking $q = r = \mu = 0$. Thus, the model

described in equation (1.1) is a more general case of equation (1.3). For a more practical implementation of the above problem, the reader can refer to [24, 25].

Such phenomena can also occur in the field of viscoelastic dynamical systems, where the coefficient $p(x)$ demonstrates the Newtonian contribution to the viscosity and the integral term occurs due to viscoelasticity. To illustrate this, let us consider the generalized version of the fractional-order viscoelastic model [2, 26]

$$\sigma(x, t) + \varrho_\epsilon^\alpha \partial_t^\alpha \sigma(x, t) = E_0 \left(\epsilon(x, t) + \varrho_\sigma^\beta \partial_t^\beta \epsilon(x, t) \right), \quad \alpha < \beta, \quad (1.4)$$

where σ , ϵ denote the stress and strain, respectively. E_0 is the prolonged modulus of the elasticity. ϱ_ϵ and ϱ_σ represent the relaxation and retardation times, respectively. Further, α , β are the orders of the fractional operators that lie between 0 and 1. Model (1.4) represents instantaneous elasticity and describes wave processes because $\alpha < \beta$ whereas, for $\alpha = \beta$, it lacks instantaneous elasticity and describes diffusion processes. Now, applying \mathfrak{J}^α on both sides of (1.4) yields

$$\partial_t^\gamma \epsilon(x, t) + \frac{1}{\varrho_\sigma^\beta \Gamma(\alpha)} \int_0^t (t-s)^{\alpha-1} \epsilon(x, s) ds = \mathcal{F}(x, t), \quad (1.5)$$

where $\gamma = \beta - \alpha \in (0, 1)$, and $\mathcal{F}(x, t) = \frac{\varrho_\epsilon^\alpha}{E_0 \varrho_\sigma^\beta} \sigma(x, t) + \frac{1}{E_0 \varrho_\sigma^\beta \Gamma(\alpha)} \int_0^t (t-s)^{\alpha-1} \sigma(x, s) ds$. Here, the stress σ is considered to be known with $\sigma(x, 0) = 0$, and the strain function ϵ is unknown that satisfies the initial condition $\epsilon(x, 0) = 0$. Note that (1.5) can be obtained by setting $p = q = r = 0$ in model (1.1). Thus, the present problems described in (1.1) and (1.2) are a more general version of (1.3) and (1.5) in the context of fractional-order integro-partial differential equations having memory effects due to which the convergence analysis will be a challenging task.

Several attempts have been made to develop accurate, stable, and high-order approximations for fractional derivatives. Among them, the $L1$ discretization is a good approximation, which has been widely used in [27, 19], for fractional problems having initial weak singularities. The method provides first-order convergence on any subdomain away from the origin, whereas it produces a lower rate of convergence over the entire region (this phenomenon is highlighted in [5, 28]). Even though the nonuniform mesh is more effective than the uniform mesh in capturing the initial layer, it fails to occur with second-order accuracy [29]. Furthermore, considering the higher regularity assumption for the solution of the fractional problems, the $L1$ discretization gives $O((\Delta t)^{2-\alpha})$ accuracy [20], where Δt denotes the step length in the time direction. In an attempt to develop high-order accuracy, Gao *et al.* [30] developed an efficient approximation called $L1-2$ scheme, which gives $O((\Delta t)^{3-\alpha})$ temporal accuracy at t_n ($n \geq 2$) but at t_1 , it produces $O((\Delta t)^{2-\alpha})$ convergence rate. In contrast, Alikhanov [31] constructed $L2-1_\sigma$ scheme that generates a temporal accuracy $O((\Delta t)^{3-\alpha})$ for all t_n ($n \geq 1$).

To the best of our knowledge, there is no work available in the literature that uses wavelet decomposition and $L2-1_\sigma$ scheme to construct a higher-order numerical approximation in the context of one and two-dimensional TFIPDEs involving convection-diffusion-reaction terms. The major contributions of the present study are highlighted as follows:

- The present work not only deals with the higher-order numerical approximation of the generalized version of convection-diffusion-reaction TFIPDEs for a sufficiently smooth solution but also applies the method to solve higher-dimensional TFIPDEs.
- Qualitative analysis in terms of the existence and uniqueness of the proposed models is new under the desired conditions.
- The multi-resolution analysis of the given wavelet decomposition method together with the $L2-1_\sigma$ scheme is fully novel in the context of two-dimensional TFIPDEs (see Lemma 4.7, Theorems 4.8 and 4.9).
- The physical effects of each term, including fractional operators, convection-diffusion-reaction terms, and integral operators have been analyzed in detail (see Theorems 4.3 and 4.10, Notes 2 and 4).
- In contrast to certain existing approaches, the proposed technique offers qualitative analysis, theoretical predictions, and experimental support for higher-order accuracy in space-time for TFIPDEs in one and two dimensions.

The remainder of the paper is organized as follows. We start with the analytical properties of the present research problems in Section 2, where we have shown the existence and uniqueness criteria of the proposed models (Problem I, Problem II); in particular, the Schauder fixed point theorem is taken into account to show the existence of solutions with the required conditions. Then, the $L2-1_\sigma$ scheme is proposed in Section 3 to discretize the fractional temporal operator to obtain a higher-order temporal accuracy for the approximation of the proposed TFIPDEs. A repeated quadrature rule based on trapezoidal approximation is employed to discretize the Volterra operator, whereas a centrally approximated second-order scheme is used to discretize the spatial derivatives for Problem I. A two-dimensional wavelet decomposition method based on Haar wavelets is proposed for grid adaption in the spatial direction to approximate Problem II. The stability and convergence analysis in the context of wavelet approximation are discussed in Section 4. It can be observed that the proposed scheme provides a higher-order accuracy (possibly second-order) in the space-time domain. Section 5 demonstrates the theoretical validation by experimenting with the proposed scheme on numerous examples of types (1.1) and (1.2). Further, we compare our desired higher-order accuracy with the results obtained by the $L1$ scheme applied to TFIPDEs through several graphs and tables. The concluding remarks are presented in Section 6.

Notation: Throughout this paper, we denote C as a generic positive constant independent of the mesh parameter, which can take different values at different places. Furthermore, $C_{x,t}^{4,3}(\bar{\Omega}, \mathbb{R})$ represents the space of all real-valued functions whose fourth and third derivatives with respect to x and t , respectively, exist and

are continuous. Then, for any $\mathcal{V} \in C_{x,t}^{4,3}(\bar{\Omega}, \mathbb{R})$, we define:

$$\|\mathcal{V}\|_{C_{x,t}^{4,3}(\bar{\Omega})} := \|\mathcal{V}\|_{\infty} + \sum_{j=1}^3 \left\| \frac{\partial^j \mathcal{V}}{\partial t^j} \right\|_{\infty} + \sum_{j=1}^4 \left\| \frac{\partial^j \mathcal{V}}{\partial x^j} \right\|_{\infty},$$

where, $\|\cdot\|_{\infty}$ denotes the usual sup-norm defined by: $\|\mathcal{V}\|_{\infty} := \sup_{(x,t) \in \bar{\Omega}} |\mathcal{V}|$.

2. The materialization of analytical quality

120 In this section, we show the existence and uniqueness of the solution to model problems (1.1) and (1.2) in the spaces $C_{x,t}^{4,3}(\bar{\Omega}, \mathbb{R})$ and $C_{\mathbf{x},t}^{4,3}(\bar{\mathcal{G}} \times [0, T], \mathbb{R})$, respectively, where $C_{\mathbf{x},t}^{4,3}(\bar{\mathcal{G}} \times [0, T], \mathbb{R})$ denote the space of all real-valued functions, whose fourth derivatives with respect to x, y including mixed derivatives, and third derivative with respect to t , exist and are continuous. The main purpose of assuming a higher regularity in the temporal variable is to obtain a higher-order accuracy in the time-space domain (the physical effect can
125 be seen in Theorems 4.3 and 4.5). The consequences of taking such a higher regularity assumption in the solution imply that the solutions of the proposed models lie in a subclass of (1.1) and (1.2) depending on the initial data [32]. The following lemma is used in Theorem 2.2 to establish the existence and uniqueness criteria, which reveals that the initial data can not be chosen freely for such a higher regularity assumption.

Lemma 2.1. *Suppose that the solution of the proposed model (1.1) lies in $C_{x,t}^{4,3}(\bar{\Omega}, \mathbb{R})$, then the initial data
130 satisfy:*

$$-\mathcal{L}g(x) = f(x, 0), \text{ for } x \in [0, L]. \quad (2.1)$$

Proof. Note that $|\partial_t^\alpha \mathcal{U}(x, t)| \leq \frac{1}{\Gamma(1-\alpha)} \int_0^t (t-s)^{-\alpha} |\mathcal{U}_s(x, s)| ds \leq \frac{Ct^{1-\alpha}}{\Gamma(\alpha)} \rightarrow 0$ as $t \rightarrow 0$. Consequently, we have $\lim_{t \rightarrow 0} \partial_t^\alpha \mathcal{U}(x, t) = 0$. The result then follows from (1.1). \square

Notice that the linear operator $\mathcal{T} \equiv \frac{d^2}{dx^2}$ is not bounded on $C(\bar{\Omega})$ even the the function \mathcal{U} is in $C^3(\bar{\Omega})$. For instance, if we take $\mathcal{U}_n = x^n$, $x \in (0, 1)$ which is bounded on $[0, 1]$ but $\mathcal{T}\mathcal{U}_n = n(n-1)x^{n-2}$ is blowing up as
135 $n \rightarrow \infty$. For this reason, the usual Banach fixed point theorem does not guarantee the existence of a unique solution for the given models (1.1) and (1.2). Special care must be taken to demonstrate their existence and uniqueness. Apply \mathfrak{J}^α on both sides of (1.1) to obtain

$$\begin{aligned} \mathcal{U}(x, t) = & g(x) + p(x)\mathfrak{J}^\alpha \left[\frac{\partial^2 \mathcal{U}}{\partial x^2} \right] - q(x)\mathfrak{J}^\alpha \left[\frac{\partial \mathcal{U}}{\partial x} \right] - r(x)\mathfrak{J}^\alpha [\mathcal{U}(x, t)] - \mathfrak{J}^\alpha \left[\mu \int_0^t \mathcal{K}(x, t-\xi) \mathcal{U}(x, \xi) d\xi \right] \\ & + \mathfrak{J}^\alpha [f(x, t)]. \end{aligned} \quad (2.2)$$

Theorem 2.2. *Given that the functions p, q, r, f, g and kernel \mathcal{K} are sufficiently smooth with $p_{xx} \leq 0$, $q_x \leq 0$, and the initial data g satisfies (2.1), the existence of a unique solution $\mathcal{U} \in C_{x,t}^{4,3}(\bar{\Omega}, \mathbb{R})$ to the given problem
140 (1.1) can be guaranteed.*

Proof. The condition upon initial data described in Lemma 2.1 allows us to define an operator $\mathbf{F} : C_{x,t}^{4,3}(\bar{\Omega}, \mathbb{R}) \rightarrow C_{x,t}^{4,3}(\bar{\Omega}, \mathbb{R})$ such that

$$\begin{aligned} \mathbf{F}\mathcal{U}(x, t) = & g(x) + p(x)\mathfrak{J}^\alpha \left[\frac{\partial^2 \mathcal{U}}{\partial x^2} \right] - q(x)\mathfrak{J}^\alpha \left[\frac{\partial \mathcal{U}}{\partial x} \right] - r(x)\mathfrak{J}^\alpha [\mathcal{U}(x, t)] - \mathfrak{J}^\alpha \left[\mu \int_0^t \mathcal{K}(x, t - \xi) \mathcal{U}(x, \xi) d\xi \right] \\ & + \mathfrak{J}^\alpha [f(x, t)]. \end{aligned}$$

Then, from (2.2), we have $\mathcal{U}(x, t) = \mathbf{F}\mathcal{U}(x, t)$, for $(x, t) \in \bar{\Omega}$. To show \mathbf{F} is compact, we must prove $\{\mathbf{F}u_n\}$ is bounded and equicontinuous [33] on $C_{x,t}^{4,3}(\bar{\Omega}, \mathbb{R})$ for any bounded sequence $\{u_n\}$ in $C_{x,t}^{4,3}(\bar{\Omega}, \mathbb{R})$. Then, the
145 Arzela-Ascoli's theorem [34] confirms the existence of a uniformly convergent subsequence of $\{\mathbf{F}u_n\}$ with respect to the norm $\|\cdot\|_\infty$.

Let us take $\|\cdot\|_\infty$ on both sides of the above equation and then apply the triangle inequality to obtain:

$$\begin{aligned} \|\mathbf{F}\mathcal{U}_n\|_\infty \leq & \|g\|_\infty + \|p\|_\infty \mathfrak{J}^\alpha \left[\left\| \frac{\partial^2 \mathcal{U}_n}{\partial x^2} \right\|_\infty \right] + \|q\|_\infty \mathfrak{J}^\alpha \left[\left\| \frac{\partial \mathcal{U}_n}{\partial x} \right\|_\infty \right] + \|r\|_\infty \mathfrak{J}^\alpha [\|\mathcal{U}_n\|_\infty] \\ & + \mathfrak{J}^\alpha \left[\mu \int_0^t \|\mathcal{K}\|_\infty \|\mathcal{U}_n\|_\infty d\xi \right] + \mathfrak{J}^\alpha [\|f(x, t)\|_\infty] \\ \leq & \|g\|_\infty + \frac{T^\alpha [(\alpha + 1)(\|p\|_\infty + \|q\|_\infty + \|r\|_\infty) + T\mu\|\mathcal{K}\|_\infty]}{\Gamma(\alpha + 2)} \|\mathcal{U}_n\|_{C_{x,t}^{4,3}(\bar{\Omega})} + \frac{\|f\|_\infty T^\alpha}{\Gamma(\alpha + 1)}. \end{aligned}$$

Notice that the functions p, q, r, g, f and kernel \mathcal{K} are sufficiently smooth functions, and $\{\mathcal{U}_n\}$ is bounded in $C_{x,t}^{4,3}(\bar{\Omega}, \mathbb{R})$. Hence, there exists a real number $\mathfrak{M}_1 > 0$ such that $\|\mathbf{F}\mathcal{U}_n\|_\infty \leq \mathfrak{M}_1$ for all $n \in \mathbb{N}$, $(x, t) \in \bar{\Omega}$.

150 This proves that $\{\mathbf{F}\mathcal{U}_n\}$ is bounded. Further, let $\epsilon > 0$ be given. For any $\mathcal{U}_n \in C_{x,t}^{4,3}(\bar{\Omega}, \mathbb{R})$, consider

$$\begin{aligned} \left| \mathbf{F}\mathcal{U}_n(x, t) - \mathbf{F}\mathcal{U}_n(y, t) \right| \leq & |g(x) - g(y)| + |p(x)|\mathfrak{J}^\alpha \left[\left| \frac{\partial^2 \mathcal{U}_n}{\partial x^2}(x, t) - \frac{\partial^2 \mathcal{U}_n}{\partial x^2}(y, t) \right| \right] \\ & + |p(x) - p(y)|\mathfrak{J}^\alpha \left[\left| \frac{\partial^2 \mathcal{U}_n}{\partial x^2}(y, t) \right| \right] + |q(x)|\mathfrak{J}^\alpha \left[\left| \frac{\partial \mathcal{U}_n}{\partial x}(x, t) - \frac{\partial \mathcal{U}_n}{\partial x}(y, t) \right| \right] \\ & + |q(x) - q(y)|\mathfrak{J}^\alpha \left[\left| \frac{\partial \mathcal{U}_n}{\partial x}(y, t) \right| \right] + |r(x)|\mathfrak{J}^\alpha [|\mathcal{U}_n(x, t) - \mathcal{U}_n(y, t)|] \\ & + |r(x) - r(y)|\mathfrak{J}^\alpha [|\mathcal{U}_n(y, t)|] + \mathfrak{J}^\alpha \left[\mu \int_0^t (|\mathcal{K}||\mathcal{U}_n(x, \xi) - \mathcal{U}_n(y, \xi)| \right. \\ & \left. + |\mathcal{K}(x, t - \xi) - \mathcal{K}(y, t - \xi)| |\mathcal{U}_n(y, \xi)|) d\xi \right] + \mathfrak{J}^\alpha [|f(x, t) - f(y, t)|]. \end{aligned}$$

Lagrange's Mean Value theorem yields the following

$$\begin{aligned} \left| \mathbf{F}\mathcal{U}_n(x, t) - \mathbf{F}\mathcal{U}_n(y, t) \right| \leq & |x - y| |g'(\theta_1)| + \frac{|x - y| T^\alpha}{\Gamma(\alpha + 1)} \left(|p(x)| \left| \frac{\partial^3 \mathcal{U}_n}{\partial x^3}(\theta_2, t) \right| + |p'(\theta_3)| \left| \frac{\partial^2 \mathcal{U}_n}{\partial x^2}(y, t) \right| \right) \\ & + \frac{|x - y| T^\alpha}{\Gamma(\alpha + 1)} \left(|q(x)| \left| \frac{\partial^2 \mathcal{U}_n}{\partial x^2}(\theta_4, t) \right| + |q'(\theta_5)| \left| \frac{\partial \mathcal{U}_n}{\partial x}(y, t) \right| \right) \\ & + \frac{|x - y| T^\alpha}{\Gamma(\alpha + 1)} \left(|r(x)| \left| \frac{\partial \mathcal{U}_n}{\partial x}(\theta_6, t) \right| + |r'(\theta_7)| |\mathcal{U}_n(y, t)| \right) \\ & + \frac{|x - y| \mu T^{\alpha+1}}{\Gamma(\alpha + 2)} \left(|\mathcal{K}| \left| \frac{\partial \mathcal{U}_n}{\partial x}(\theta_8, \xi) \right| + \left| \frac{\partial \mathcal{K}}{\partial x}(\theta_9, t - \xi) \right| |\mathcal{U}_n(y, \xi)| \right) \\ & + \frac{|x - y| T^\alpha}{\Gamma(\alpha + 1)} \left| \frac{\partial f}{\partial x}(\theta_{10}, t) \right|, \end{aligned}$$

where $x < \theta_i < y$ for $i = 1, 2, \dots, 10$. Notice that, $p, q, r, f, g, \mathcal{K}$ are sufficiently smooth, and $\mathcal{U}_n \in C_{x,t}^{4,3}(\bar{\Omega}, \mathbb{R})$. Hence we have

$$\left| \mathbf{F}\mathcal{U}_n(x, t) - \mathbf{F}\mathcal{U}_n(y, t) \right| \leq |x - y| \mathfrak{M}_2,$$

where \mathfrak{M}_2 is the upper bound of the right-hand side expression sans the factor $|x - y|$. Let us choose
155 $\delta = \min \left\{ \epsilon, \frac{\epsilon}{\mathfrak{M}_2} \right\}$, and take $|x - y| < \delta$ to yield

$$\left| \mathbf{F}\mathcal{U}_n(x, t) - \mathbf{F}\mathcal{U}_n(y, t) \right| < \epsilon, \quad \text{for all } n \in \mathbb{N}, \quad t \in (0, T].$$

Hence, $\{\mathbf{F}\mathcal{U}_n\}$ is equicontinuous. Therefore, by the Arzela-Ascoli's theorem, $\{\mathbf{F}\mathcal{U}_n\}$ has a subsequence that converges uniformly and hence converges with respect to the norm $\|\cdot\|_\infty$. Subsequently, the Schauder fixed point theorem [35] confirms the existence of a solution $\mathcal{U} \in C_{x,t}^{4,3}(\bar{\Omega}, \mathbb{R})$ for (1.1).

To prove the unicity, let $\mathcal{U}_1, \mathcal{U}_2$ be two solutions of (1.1), Then $\mathcal{W} = \mathcal{U}_1 - \mathcal{U}_2$ will be a solution of

$$\begin{cases} \partial_t^\alpha \mathcal{W}(x, t) - \mathcal{L}\mathcal{W}(x, t) + \mu \int_0^t \mathcal{K}(x, t - \xi) \mathcal{W}(x, \xi) d\xi = 0, & (x, t) \in \Omega, \\ \mathcal{W}(x, 0) = 0 \text{ for } x \in [0, L], \quad \mathcal{W}(0, t) = \mathcal{W}(1, t) = 0 \text{ for } t \in (0, T]. \end{cases}$$

160 Our aim is to show that \mathcal{W} is identically zero. Let us take $\mathcal{W} = \mathcal{W}^+ - \mathcal{W}^-$, with $\mathcal{W}^+ := \max\{0, \mathcal{W}\}$ and $\mathcal{W}^- := \max\{0, -\mathcal{W}\}$.

$$\begin{aligned} \int_0^L \partial_t^\alpha (\mathcal{W}^+ - \mathcal{W}^-) \mathcal{W}^+ dx &= \int_0^L p(\mathcal{W}_{xx}^+ - \mathcal{W}_{xx}^-) \mathcal{W}^+ dx - \int_0^L q(\mathcal{W}_x^+ - \mathcal{W}_x^-) \mathcal{W}^+ dx \\ &\quad - \int_0^L r(\mathcal{W}^+ - \mathcal{W}^-) \mathcal{W}^+ dx - \int_0^L \left(\mu \int_0^t \mathcal{K}(\mathcal{W}^+ - \mathcal{W}^-) d\xi \right) \mathcal{W}^+ dx. \end{aligned}$$

Integrating by parts and a simple calculation gives

$$\begin{aligned} \int_0^L (\partial_t^\alpha \mathcal{W}^+) \mathcal{W}^+ dx &= \frac{1}{2} \int_0^L p_{xx} (\mathcal{W}^+)^2 dx - \int_0^L p (\mathcal{W}_x^+)^2 dx + \frac{1}{2} \int_0^L q_x (\mathcal{W}^+)^2 dx \\ &\quad - \int_0^L r (\mathcal{W}^+)^2 dx - \int_0^L \left(\mu \int_0^t \mathcal{K} \mathcal{W}^+ d\xi \right) \mathcal{W}^+ dx. \end{aligned}$$

Notice that $\mathcal{W}^+ \geq 0$. Under the assumption that $p_{xx} \leq 0$, $q_x \leq 0$, the right-hand side of the above expression is ≤ 0 . This yields $\partial_t^\alpha \mathcal{W}^+ \leq 0$, which implies $\mathcal{W}_t^+ \leq 0$. Subsequently, \mathcal{W}^+ decreases as t increases with
165 $\mathcal{W}^+(x, 0) = 0$. This is only possible when $\mathcal{W}^+ = 0$. In a similar way, it can be proved that $\mathcal{W}^- = 0$. Therefore $\mathcal{W} \equiv 0$ and hence $\mathcal{U}_1 \equiv \mathcal{U}_2$. \square

The following theorem demonstrates the existence and uniqueness of the solution of the two-dimensional TFIPDEs (1.2).

Theorem 2.3. *Given that the functions $p_1, p_2, q_1, q_2, r_1, f, g$ and kernel \mathcal{K} are sufficiently smooth with
170 $(p_1)_{xx}, (p_2)_{xx} \leq 0$, $(q_1)_x, (q_2)_x \leq 0$, the existence of a unique solution $\mathcal{U} \in C_{x,t}^{4,3}(\bar{\mathcal{G}} \times [0, T], \mathbb{R})$ to the given problem (1.2) can be guaranteed provided the initial data satisfy (2.1) over $\bar{\mathcal{G}}$ with respect to the operator \mathfrak{L} .*

Proof. This theorem can be proved in a similar way as described in Theorem 2.2. \square

3. Numerical methods

This section comprises the procedure of the construction of the numerical schemes to solve the one and two-dimensional fractional integro-PDEs depicted in (1.1) and (1.2).

3.1. Approximation of one-dimensional TFIPDEs

To solve the one-dimensional integro-PDEs (1.1), we approximate the Caputo derivative by $L2-1_\sigma$ scheme, the spatial derivatives are discretized by central difference operators, and the composite trapezoidal formula is used to deal with the Volterra integral operator. Let $M, N \in \mathbb{N}$ be fixed. Set: $\Delta x = L/M, \Delta t = T/N$. The mesh points are defined as $x_m = m\Delta x, t_n = n\Delta t, m = 0, 1, \dots, M; n = 0, 1, \dots, N$. Thus, the discrete domain is given by: $\Omega_{M,N} := \{(x_m, t_n) : m = 0, 1, \dots, M; n = 0, 1, \dots, N\}$. Suppose $\{\mathcal{U}_m^n\}_{m=0, n=0}^{M,N}$ denote the mesh function approximating $\mathcal{U}(x, t)$ at each (x_m, t_n) . Further, we denote $t_{n+\sigma} = t_n + \sigma\Delta t$ for some constant $\sigma \in (0, 1)$. At the mesh point $(x_m, t_{n+\sigma})$, the fractional Caputo derivative is redefined as:

$$\begin{aligned}\partial_t^\alpha \mathcal{U}(x_m, t_{n+\sigma}) &= \frac{1}{\Gamma(1-\alpha)} \int_{t_0}^{t_{n+\sigma}} (t_{n+\sigma} - \rho)^{-\alpha} \mathcal{U}_\rho(x_m, \rho) d\rho \\ &= \frac{1}{\Gamma(1-\alpha)} \left(\sum_{j=1}^n \int_{t_{j-1}}^{t_j} (t_{n+\sigma} - \rho)^{-\alpha} \mathcal{U}_\rho(x_m, \rho) d\rho + \int_{t_n}^{t_{n+\sigma}} (t_{n+\sigma} - \rho)^{-\alpha} \mathcal{U}_\rho(x_m, \rho) d\rho \right)\end{aligned}$$

The basic idea of $L2-1_\sigma$ formula is that the function $\mathcal{U}(x_m, t)$ is approximated by a quadratic interpolation $\mathcal{P}_{2,n}(x_m, t)$ over the interval $(t_{n-1}, t_n), n = 1, 2, \dots, N-1$ and in the interval $(t_n, t_{n+1}), n = 0, 1, \dots, N-1$, it is approximated by a linear interpolation $\mathcal{P}_{1,n}(x_m, t)$. The interpolations are defined as:

$$\begin{cases} \mathcal{P}_{2,n}(x_m, t) = \frac{(t - t_n)(t - t_{n+1})}{2(\Delta t)^2} \mathcal{U}_m^{n-1} - \frac{(t - t_{n-1})(t - t_{n+1})}{(\Delta t)^2} \mathcal{U}_m^n + \frac{(t - t_{n-1})(t - t_n)}{2(\Delta t)^2} \mathcal{U}_m^{n+1}, \\ \mathcal{P}_{1,n}(x_m, t) = \frac{t_{n+1} - t}{\Delta t} \mathcal{U}_m^n + \frac{t - t_n}{\Delta t} \mathcal{U}_m^{n+1}. \end{cases}$$

Differentiating with respect to t we have

$$\begin{cases} \mathcal{P}'_{2,n}(x_m, t) = \left(\frac{t_{n+\frac{1}{2}} - t}{\Delta t} \right) \left(\frac{\mathcal{U}_m^n - \mathcal{U}_m^{n-1}}{\Delta t} \right) + \left(\frac{t - t_{n-\frac{1}{2}}}{\Delta t} \right) \left(\frac{\mathcal{U}_m^{n+1} - \mathcal{U}_m^n}{\Delta t} \right), \\ \mathcal{P}'_{1,n}(x_m, t) = \frac{\mathcal{U}_m^{n+1} - \mathcal{U}_m^n}{\Delta t}. \end{cases}$$

Hence, we have the following discretization for fractional Caputo derivative:

$$\begin{aligned}\partial_t^\alpha \mathcal{U}(x_m, t_{n+\sigma}) &\approx {}^{L2-1_\sigma} \mathcal{D}_N^\alpha \mathcal{U}_m^{n+\sigma} := \frac{1}{\Gamma(1-\alpha)} \left(\sum_{j=1}^n \int_{t_{j-1}}^{t_j} (t_{n+\sigma} - \rho)^{-\alpha} \mathcal{P}'_{2,n}(x_m, \rho) d\rho + \int_{t_n}^{t_{n+\sigma}} (t_{n+\sigma} - \rho)^{-\alpha} \mathcal{P}'_{1,n}(x_m, \rho) d\rho \right) \\ &= \sum_{j=0}^n d_j^{n+1} (\mathcal{U}_m^{j+1} - \mathcal{U}_m^j).\end{aligned}\tag{3.1}$$

Here, $d_0^1 = \frac{a_0}{(\Delta t)^\alpha \Gamma(2-\alpha)}$, and for $n \geq 1$

$$d_j^{n+1} = \frac{1}{(\Delta t)^\alpha \Gamma(2-\alpha)} \begin{cases} a_n - b_n, & j = 0, \\ b_{n-j+1} + a_{n-j} - b_{n-j}, & 1 \leq j \leq n-1, \\ a_0 + b_1, & j = n, \end{cases}\tag{3.2}$$

190 with $a_0 = \sigma^{1-\alpha}$, $a_k = (k + \sigma)^{1-\alpha} - (k - 1 + \sigma)^{1-\alpha}$, $k \geq 1$, and $b_k = \frac{1}{2-\alpha} [(k + \sigma)^{2-\alpha} - (k - 1 + \sigma)^{2-\alpha}] - \frac{1}{2} [(k + \sigma)^{1-\alpha} + (k - 1 + \sigma)^{1-\alpha}]$, $k \geq 1$. The following lemma helps to discretize the spatial derivatives as well as to estimate the truncation error bound for the proposed schemes.

Lemma 3.1. *For any $\phi(t) \in C^2([0, T])$, and $n = 0, 1, \dots, N - 1$, we have*

$$\phi(t_{n+\sigma}) = \sigma\phi(t_{n+1}) + (1 - \sigma)\phi(t_n) + O((\Delta t)^2), \quad \sigma \in (0, 1).$$

Proof. Using the Taylor series expansion, one can easily verify the result. \square

195 Based on Lemma 3.1, we have the following approximation of \mathcal{U}_{xx} and \mathcal{U}_x .

$$\begin{aligned} \mathcal{U}_{xx}(x_m, t_{n+\sigma}) &= \sigma\mathcal{U}_{xx}(x_m, t_{n+1}) + (1 - \sigma)\mathcal{U}_{xx}(x_m, t_n) + O((\Delta t)^2) \\ &\approx \frac{\sigma}{(\Delta x)^2} (\mathcal{U}_{m-1}^{n+1} - 2\mathcal{U}_m^{n+1} + \mathcal{U}_{m+1}^{n+1}) + \frac{1-\sigma}{(\Delta x)^2} (\mathcal{U}_{m-1}^n - 2\mathcal{U}_m^n + \mathcal{U}_{m+1}^n) + O((\Delta t)^2 + (\Delta x)^2) \\ &= \delta_{\Delta x, \Delta t}^2 \mathcal{U}_m^{n+\sigma} + O((\Delta t)^2 + (\Delta x)^2), \end{aligned} \quad (3.3)$$

provided $\mathcal{U} \in C_{x,t}^{4,3}(\bar{\Omega}, \mathbb{R})$, where

$$\delta_{\Delta x, \Delta t}^2 \mathcal{U}_m^{n+\sigma} = \frac{\sigma}{h^2} (\mathcal{U}_{m-1}^{n+1} - 2\mathcal{U}_m^{n+1} + \mathcal{U}_{m+1}^{n+1}) + \frac{1-\sigma}{h^2} (\mathcal{U}_{m-1}^n - 2\mathcal{U}_m^n + \mathcal{U}_{m+1}^n).$$

Further,

$$\begin{aligned} \mathcal{U}_x(x_m, t_{n+\sigma}) &= \sigma\mathcal{U}_x(x_m, t_{n+1}) + (1 - \sigma)\mathcal{U}_x(x_m, t_n) + O((\Delta t)^2) \\ &\approx \frac{\sigma}{2\Delta x} (\mathcal{U}_{m+1}^{n+1} - \mathcal{U}_{m-1}^{n+1}) + \frac{1-\sigma}{2\Delta x} (\mathcal{U}_{m+1}^n - \mathcal{U}_{m-1}^n) + O((\Delta t)^2 + (\Delta x)^2) \\ &= D_{\Delta x, \Delta t}^0 \mathcal{U}_m^{n+\sigma} + O((\Delta t)^2 + (\Delta x)^2), \end{aligned} \quad (3.4)$$

where $D_{\Delta x, \Delta t}^0 \mathcal{U}_m^{n+\sigma} = \frac{\sigma}{2\Delta x} (\mathcal{U}_{m+1}^{n+1} - \mathcal{U}_{m-1}^{n+1}) + \frac{1-\sigma}{2\Delta x} (\mathcal{U}_{m+1}^n - \mathcal{U}_{m-1}^n)$. We now discretize the Volterra integral operator as follows:

$$\begin{aligned} \int_0^{t_{n+\sigma}} \mathcal{K}(x_m, t_{n+\sigma} - \xi) \mathcal{U}(x_m, \xi) d\xi &= \sum_{j=0}^{n-1} \int_{t_j}^{t_{j+1}} \mathcal{K}(x_m, t_{n+\sigma} - \xi) \mathcal{U}(x_m, \xi) d\xi \\ &\quad + \int_{t_n}^{t_{n+\sigma}} \mathcal{K}(x_m, t_{n+\sigma} - \xi) \mathcal{U}(x_m, \xi) d\xi \\ &= \frac{\Delta t}{2} \sum_{j=0}^{n-1} [\mathcal{K}(x_m, t_{n+\sigma} - t_{j+1}) \mathcal{U}(x_m, t_{j+1}) + \mathcal{K}(x_m, t_{n+\sigma} - t_j) \mathcal{U}(x_m, t_j)] \\ &\quad + \frac{\sigma \Delta t}{2} [\mathcal{K}(x_m, t_{n+\sigma} - t_n) \mathcal{U}(x_m, t_n) + \mathcal{K}(x_m, 0) \mathcal{U}(x_m, t_{n+\sigma})] + O((\Delta t)^2) \\ &\approx \frac{\Delta t}{2} \sum_{j=0}^{n-1} [\mathcal{K}(x_m, t_{n+\sigma} - t_{j+1}) \mathcal{U}_m^{j+1} + \mathcal{K}(x_m, t_{n+\sigma} - t_j) \mathcal{U}_m^j] + \frac{\sigma \Delta t}{2} \mathcal{K}(x_m, t_{n+\sigma} - t_n) \mathcal{U}_m^n \\ &\quad + \frac{\sigma \Delta t}{2} \mathcal{K}(x_m, 0) [\sigma \mathcal{U}_m^{n+1} + (1 - \sigma) \mathcal{U}_m^n] + O((\Delta t)^2) \\ &= \mathcal{J}_N \mathcal{U}_m^{n+\sigma} + O((\Delta t)^2), \end{aligned} \quad (3.5)$$

where

$$\begin{aligned}\mathcal{J}_N \mathcal{U}_m^{n+\sigma} &= \frac{\Delta t}{2} \sum_{j=0}^{n-1} [\mathcal{K}(x_m, t_{n+\sigma} - t_{j+1}) \mathcal{U}_m^{j+1} + \mathcal{K}(x_m, t_{n+\sigma} - t_j) \mathcal{U}_m^j] \\ &\quad + \frac{\sigma \Delta t}{2} \mathcal{K}(x_m, t_{n+\sigma} - t_n) \mathcal{U}_m^n + \frac{\sigma \Delta t}{2} \mathcal{K}(x_m, 0) [\sigma \mathcal{U}_m^{n+1} + (1 - \sigma) \mathcal{U}_m^n].\end{aligned}$$

200 Based on the above discretizations discussed in (3.1)–(3.5), we have

$$\left\{ \begin{array}{l} {}^{L2-1\sigma} \mathcal{D}_N^\alpha \mathcal{U}(x_m, t_{n+\sigma}) - p(x_m) \delta_{\Delta x, \Delta t}^2 \mathcal{U}(x_m, t_{n+\sigma}) + q(x_m) D_{\Delta x, \Delta t}^0 \mathcal{U}(x_m, t_{n+\sigma}) \\ \quad + r(x_m) \mathcal{U}(x_m, t_{n+\sigma}) + \mu \mathcal{J}_N \mathcal{U}(x_m, t_{n+\sigma}) = f(x_m, t_{n+\sigma}) + {}^{L2-1\sigma} \mathcal{R}_m^{n+\sigma}, \\ \text{for } m = 1, 2, \dots, M-1; \ n = 0, 1, \dots, N-1, \\ \mathcal{U}(x_m, t_0) = g(x_m) \text{ for } m = 0, 1, \dots, M, \\ \mathcal{U}(x_0, t_n) = h_1(t_n) \text{ and } \mathcal{U}(x_M, t_n) = h_2(t_n) \text{ for } n = 0, 1, \dots, N. \end{array} \right. \quad (3.6)$$

${}^{L2-1\sigma} \mathcal{R}_m^{n+\sigma}$ is the remainder term given by

$${}^{L2-1\sigma} \mathcal{R}_m^{n+\sigma} = \left(\partial_t^\alpha - {}^{L2-1\sigma} \mathcal{D}_N^\alpha \right) \mathcal{U}(x_m, t_{n+\sigma}) + O((\Delta t)^2 + (\Delta x)^2). \quad (3.7)$$

Hence, the discrete version of (1.1) can be obtained as:

$$\left\{ \begin{array}{l} {}^{L2-1\sigma} \mathcal{D}_N^\alpha \mathcal{U}_m^{n+\sigma} - p(x_m) \delta_{\Delta x, \Delta t}^2 \mathcal{U}_m^{n+\sigma} + q(x_m) D_{\Delta x, \Delta t}^0 \mathcal{U}_m^{n+\sigma} + r(x_m) \mathcal{U}_m^{n+\sigma} + \mu \mathcal{J}_N \mathcal{U}_m^{n+\sigma} = f(x_m, t_{n+\sigma}), \\ \text{for } m = 1, 2, \dots, M-1; \ n = 0, 1, \dots, N-1, \\ \mathcal{U}_m^0 = g(x_m) \text{ for } m = 0, 1, \dots, M, \\ \mathcal{U}_0^n = h_1(t_n) \text{ and } \mathcal{U}_M^n = h_2(t_n) \text{ for } n = 0, 1, \dots, N. \end{array} \right. \quad (3.8)$$

A simple calculation yields the following implicit scheme:

$$\left\{ \begin{array}{l} \mathcal{A}_{m-1} \mathcal{U}_{m-1}^{n+1} + \mathcal{B}_m \mathcal{U}_m^{n+1} + \mathcal{C}_{m+1} \mathcal{U}_{m+1}^{n+1} = \tilde{\mathcal{A}}_{m-1} \mathcal{U}_{m-1}^n + \tilde{\mathcal{B}}_m \mathcal{U}_m^n + \tilde{\mathcal{C}}_{m+1} \mathcal{U}_{m+1}^n + \mathcal{F}_m^n, \\ \text{for } m = 1, 2, \dots, M-1; \ n = 0, 1, \dots, N-1, \\ \mathcal{U}_m^0 = g(x_m) \text{ for } m = 0, 1, \dots, M, \\ \mathcal{U}_0^n = h_1(t_n) \text{ and } \mathcal{U}_M^n = h_2(t_n) \text{ for } n = 0, 1, \dots, N, \end{array} \right. \quad (3.9)$$

where the coefficients are given by

$$\left\{ \begin{array}{l} \mathcal{A}_{m-1} = -\frac{q(x_m)\sigma}{2\Delta x} - \frac{p(x_m)\sigma}{(\Delta x)^2}, \quad \mathcal{B}_m = d_m^{n+1} + \frac{2p(x_m)\sigma}{(\Delta x)^2} + r(x_m)\sigma + \frac{\mu\sigma^2\Delta t}{2} \mathcal{K}(x_m, 0), \\ \mathcal{C}_{m+1} = \frac{q(x_m)\sigma}{2\Delta x} - \frac{p(x_m)\sigma}{(\Delta x)^2}, \quad \tilde{\mathcal{A}}_{m-1} = \frac{q(x_m)(1-\sigma)}{2\Delta x} + \frac{p(x_m)(1-\sigma)}{(\Delta x)^2}, \\ \tilde{\mathcal{B}}_m = d_m^{n+1} - \frac{2p(x_m)(1-\sigma)}{(\Delta x)^2} - r(x_m)(1-\sigma) - \frac{\mu\Delta t}{2} \mathcal{K}(x_m, t_{n+\sigma} - t_n) \\ \quad - \frac{\mu\sigma\Delta t}{2} \mathcal{K}(x_m, t_{n+\sigma} - t_n) - \frac{\mu\Delta t\sigma(1-\sigma)}{2} \mathcal{K}(x_m, 0), \\ \tilde{\mathcal{C}}_{m+1} = -\frac{q(x_m)(1-\sigma)}{2\Delta x} + \frac{p(x_m)(1-\sigma)}{(\Delta x)^2}, \end{array} \right.$$

for $m = 1, 2, \dots, M-1; n = 0, 1, \dots, N-1$. Further, $\mathcal{F}_m^0 = f(x_m, t_\sigma)$, $\mathcal{F}_m^1 = -d_0^2(\mathcal{U}_m^1 - \mathcal{U}_m^0) - \frac{\Delta t}{2}\mathcal{K}(x_m, t_{1+\sigma} - t_0)\mathcal{U}_m^0 + f(x_m, t_{1+\sigma})$, and for $n = 2, 3, \dots, N-1$, we have

$$\begin{aligned} \mathcal{F}_m^n = & - \sum_{j=0}^{n-1} d_j^{n+1}(\mathcal{U}_m^{j+1} - \mathcal{U}_m^j) - \frac{\mu\Delta t}{2}\mathcal{K}(x_m, t_{n+\sigma} - t_{n-1})\mathcal{U}_m^{n-1} \\ & - \frac{\mu\Delta t}{2} \sum_{j=0}^{n-2} \left[\mathcal{K}(x_m, t_{n+\sigma} - t_{j+1})\mathcal{U}_m^{j+1} + \mathcal{K}(x_m, t_{n+\sigma} - t_j)\mathcal{U}_m^j \right] + f(x_m, t_{n+\sigma}). \end{aligned} \quad (3.10)$$

Notice that, at each time level n for $n = 0, 1, \dots, N-1$, the unknowns $\mathcal{U}_1^{n+1}, \mathcal{U}_2^{n+1}, \dots, \mathcal{U}_{M-1}^{n+1}$ can be solved from the implicit discrete scheme (3.9), which can be written as:

$$\mathbf{H}\mathbf{U}^{n+1} = \tilde{\mathbf{H}}\mathbf{U}^n + \mathcal{F}^n,$$

where $\mathbf{U}^{n+1} = (\mathcal{U}_1^{n+1}, \mathcal{U}_2^{n+1}, \dots, \mathcal{U}_{M-1}^{n+1})^T$, $\mathbf{U}^n = (\mathcal{U}_1^n, \mathcal{U}_2^n, \dots, \mathcal{U}_{M-1}^n)^T$, $\mathcal{F}^n = (\mathcal{F}_1^n, \mathcal{F}_2^n, \dots, \mathcal{F}_{M-1}^n)^T$, and

the coefficient matrices $\mathbf{H}, \tilde{\mathbf{H}}$ are defined as:

$$\mathbf{H} = \begin{pmatrix} \mathcal{B}_1 & \mathcal{C}_2 & & & \\ \mathcal{A}_1 & \mathcal{B}_2 & \mathcal{C}_3 & & \\ & \ddots & \ddots & \ddots & \\ & & \mathcal{A}_{M-3} & \mathcal{B}_{M-2} & \mathcal{C}_{M-1} \\ & & & \mathcal{A}_{M-2} & \mathcal{B}_{M-1} \end{pmatrix}, \quad \tilde{\mathbf{H}} = \begin{pmatrix} \tilde{\mathcal{B}}_1 & \tilde{\mathcal{C}}_2 & & & \\ \tilde{\mathcal{A}}_1 & \tilde{\mathcal{B}}_2 & \tilde{\mathcal{C}}_3 & & \\ & \ddots & \ddots & \ddots & \\ & & \tilde{\mathcal{A}}_{M-3} & \tilde{\mathcal{B}}_{M-2} & \tilde{\mathcal{C}}_{M-1} \\ & & & \tilde{\mathcal{A}}_{M-2} & \tilde{\mathcal{B}}_{M-1} \end{pmatrix}.$$

The invertibility of the coefficient matrix \mathbf{H} can be guaranteed from the positivity assumption of the coefficient function $p(x) \geq p_0 > 0$ and the nonrestrictive assumption of the lower bound of the number of space partitions M , which is

$$\frac{L\|q\|_\infty}{2p_0} < M. \quad (3.11)$$

Now, we present the computational procedure for solving TFIPDEs (1.1) described in Algorithm 1.

In the following segment, we describe the discretization of (1.1) based on the $L1$ scheme in order to make a comparison with the proposed method.

3.1.1. Discretization based on $L1$ scheme

The discrete scheme based on $L1$ discretization for the given problem (1.1) can be written as:

$$\left\{ \begin{array}{l} {}^{L1}\mathcal{D}_N^\alpha \mathcal{U}_m^n - p(x_m)\delta_{\Delta x}^2 \mathcal{U}_m^n + q(x_m)D_{\Delta x}^0 \mathcal{U}_m^n + r(x_m)\mathcal{U}_m^n \\ \quad + \frac{\mu\Delta t}{2} \sum_{j=0}^{n-1} [\mathcal{K}(x_m, t_n - t_{j+1})\mathcal{U}_m^{j+1} + \mathcal{K}(x_m, t_n - t_j)\mathcal{U}_m^j] = f(x_m, t_n), \\ \text{for } m = 1, 2, \dots, M-1; n = 1, 2, \dots, N, \text{ with} \\ \mathcal{U}_m^0 = g(x_m) \text{ for } m = 0, 1, \dots, M, \\ \mathcal{U}_0^n = h_1(t_n) \text{ and } \mathcal{U}_M^n = h_2(t_n) \text{ for } n = 0, 1, \dots, N, \end{array} \right. \quad (3.12)$$

Algorithm 1 ALGORITHM FOR THE SOLUTION OF ONE-DIMENSIONAL TFIPDEs

- 1: **Input 1:** α ▷ Order of the fractional operator
 - 2: **Input 2:** M ▷ Number of mesh interval towards space
 - 3: **Input 3:** N ▷ Number of mesh interval towards time
 - 4: **Input 4:** g, h_1, h_2 ▷ Initial and boundary conditions
 - 5: Compute $\sigma = 1 - (\alpha/2)$
 - 6: Compute $\Delta x = L/M$ and $\Delta t = T/N$ ▷ Mesh parameters
 - 7: Compute $x_m = m * \Delta x$ for $m = 0, 1, \dots, M$
 - 8: Compute $t_n = n * \Delta t$ for $n = 0, 1, \dots, N$
 - 9: Compute p and q ▷ Coefficient functions
 - 10: Compute \mathcal{K} ▷ The given kernel
 - 11: Compute f
 - 12: Compute d_0^1 and d_j^{n+1} for $n = 1, 2, \dots, N-1, j = 0, 1, \dots, n-1$ given in (3.1)
 - 13: **for** $n = 0, 1, \dots, N-1$ **do**
 - 14: Compute \mathbf{H} and $\tilde{\mathbf{H}}$
 - 15: Compute the vector \mathcal{F}^n using steps 4, 7 and the formula given in (3.10)
 - 16: Compute $\mathcal{U}^{n+1} = \mathbf{H}^{-1}(\tilde{\mathbf{H}}\mathcal{U}^n + \mathcal{F}^n)$
 - 17: **end for**
 - 18: **Output:** Obtained discrete solution \mathcal{U}_m^n for $m = 1, 2, \dots, M-1, n = 1, 2, \dots, N$
-

where

$$\begin{cases} \partial_t^\alpha \mathcal{U}(x_m, t_n) & \approx {}^{L1}\mathcal{D}_N^\alpha \mathcal{U}_m^n := \frac{1}{(\Delta t)^\alpha \Gamma(2-\alpha)} \sum_{j=0}^{n-1} (\mathcal{U}_m^{j+1} - \mathcal{U}_m^j) \tilde{d}_{n-j}, \\ \frac{\partial^2 \mathcal{U}}{\partial x^2}(x_m, t_n) & \approx \delta_{\Delta x}^2 \mathcal{U}_m^n := \frac{\mathcal{U}_{m+1}^n - 2\mathcal{U}_m^n + \mathcal{U}_{m-1}^n}{(\Delta x)^2}, \\ \frac{\partial \mathcal{U}}{\partial x}(x_m, t_n) & \approx D_{\Delta x}^0 \mathcal{U}_m^n := \frac{\mathcal{U}_{m+1}^n - \mathcal{U}_{m-1}^n}{2\Delta x}. \end{cases}$$

220 Here, $\tilde{d}_j = j^{1-\alpha} - (j-1)^{1-\alpha}$, $j \geq 1$. Further, $\int_0^{t_n} \mathcal{K}(x_m, t_n - \xi) \mathcal{U}(x_m, \xi) d\xi \approx \frac{\Delta t}{2} \sum_{j=0}^{n-1} [\mathcal{K}(x_m, t_n - t_{j+1}) \mathcal{U}(x_m, t_{j+1}) + \mathcal{K}(x_m, t_n - t_j) \mathcal{U}(x_m, t_j)]$. The discrete scheme (3.12) has the truncation error

$${}^{L1}\mathcal{R}_m^n = \left(\partial_t^\alpha - {}^{L1}\mathcal{D}_N^\alpha \right) \mathcal{U}(x_m, t_n) + O((\Delta t)^2 + (\Delta x)^2). \quad (3.13)$$

3.2. Approximation of two-dimensional TFIPDEs

In this section, we discuss the approximation scheme for two-dimensional integro-PDEs depicted in (1.2) based on the $L2-1_\sigma$ scheme and the Haar wavelets. First, we make the semi-discretization of the model
 225 by using the $L2-1_\sigma$ scheme for the fractional operator, and the composite trapezoidal approximation for the Volterra integral operator. The wavelet collocation method is then applied to solve the semi-discrete problem.

3.2.1. The temporal semi-discretization

The temporal direction is discretized uniformly as described in Section 3.1. In a similar way as defined in (3.1), the Caputo fractional operator presented in (1.2) is approximated at the nodal point $t_{n+\sigma}$ as

$$\partial_t^\alpha \mathcal{U}(\cdot, t_{n+\sigma}) \approx {}^{L2-1\sigma}\mathcal{D}_N^\alpha \mathcal{U}^{n+\sigma} := \sum_{j=0}^n d_j^{n+1} (\mathcal{U}^{j+1} - \mathcal{U}^j), \quad (3.14)$$

where d_j^{n+1} is defined in (3.2). The Volterra operator is discretized in a manner similar to that defined in (3.5), and is given by

$$\begin{aligned} \int_0^{t_{n+\sigma}} \mathcal{K}(\cdot, t_{n+\sigma} - \xi) \mathcal{U}(\cdot, \xi) d\xi &\approx \frac{\Delta t}{2} \sum_{j=0}^{n-1} [\mathcal{K}(\cdot, t_{n+\sigma} - t_{j+1}) \mathcal{U}^{j+1} + \mathcal{K}(\cdot, t_{n+\sigma} - t_j) \mathcal{U}^j] + \frac{\sigma \Delta t}{2} \mathcal{K}(\cdot, t_{n+\sigma} - t_n) \mathcal{U}^n \\ &+ \frac{\sigma \Delta t}{2} \mathcal{K}(\cdot, 0) [\sigma \mathcal{U}^{n+1} + (1 - \sigma) \mathcal{U}^n] + O((\Delta t)^2). \end{aligned} \quad (3.15)$$

Therefore, the temporal discretization of (1.2) is given by:

$$\begin{cases} \left(d_n^{n+1} + \frac{\mu \sigma^2 \Delta t}{2} \mathcal{K}(x, y, 0) \right) \mathcal{U}^{n+1}(x, y) - \mathfrak{L}^N \mathcal{U}^{n+\sigma}(x, y) = F^n(x, y), \\ \mathcal{U}^{n+\sigma}(0, y) = h_1(y, t_{n+\sigma}) \text{ and } \mathcal{U}^{n+\sigma}(1, y) = h_2(y, t_{n+\sigma}), \\ \mathcal{U}^{n+\sigma}(x, 0) = h_3(x, t_{n+\sigma}) \text{ and } \mathcal{U}^{n+\sigma}(x, 1) = h_4(x, t_{n+\sigma}) \quad \forall n = 0, 1, \dots, N-1, \end{cases} \quad (3.16)$$

where \mathfrak{L}^N and $F^n(x, y)$ are given by:

$$\begin{aligned} \mathfrak{L}^N \mathcal{U}^{n+\sigma}(x, y) &= p_1(x, y) \mathcal{U}_{xx}^{n+\sigma}(x, y) + p_2(x, y) \mathcal{U}_{yy}^{n+\sigma}(x, y) - q_1(x, y) \mathcal{U}_x^{n+\sigma}(x, y) \\ &- q_2(x, y) \mathcal{U}_y^{n+\sigma}(x, y) - r_1(x, y) \mathcal{U}^{n+\sigma}(x, y), \\ F^n(x, y) &= \left(d_n^{n+1} - \frac{\mu \sigma (1 - \sigma) \Delta t}{2} \mathcal{K}(x, y, 0) \right) \mathcal{U}^n(x, y) - \sum_{j=0}^{n-1} d_j^{n+1} (\mathcal{U}^{j+1}(x, y) - \mathcal{U}^j(x, y)) \\ &- \frac{\mu \sigma \Delta t}{2} \mathcal{K}(x, y, t_{n+\sigma} - t_n) \mathcal{U}^n(x, y) - \frac{\mu \Delta t}{2} \sum_{j=0}^{n-1} \left[\mathcal{K}(x, y, t_{n+\sigma} - t_{j+1}) \mathcal{U}^{j+1}(x, y) \right. \\ &\left. + \mathcal{K}(x, y, t_{n+\sigma} - t_j) \mathcal{U}^j(x, y) \right] + f(x, y, t_{n+\sigma}). \end{aligned}$$

The truncation error due to the semi-discretization of the given two-dimensional TFIPDEs can be expressed as:

$$\mathcal{R}_m^{n+1} = \left(\partial_t^\alpha - {}^{L2-1\sigma}\mathcal{D}_N^\alpha \right) \mathcal{U}(\cdot, t_{n+\sigma}) + O((\Delta t)^2). \quad (3.17)$$

3.2.2. Approximation of spatial derivatives based on Haar wavelets

In this segment, we present the complete solution of (1.2) by solving the semi-discretized problem given in (3.16) using Haar wavelets. The Haar wavelet [36, 37] consists of a sequence of square-shaped functions that together form a wavelet family. The mother wavelet function $\psi(x)$, and its scaling function $\phi(x)$ are defined

as follows:

$$\psi(x) = \begin{cases} 1, & \text{for } t \in \left[0, \frac{1}{2}\right), \\ -1, & \text{for } t \in \left[\frac{1}{2}, 1\right), \\ 0, & \text{elsewhere,} \end{cases} \quad \text{and} \quad \phi(x) = \begin{cases} 1, & \text{for } t \in [0, 1), \\ 0, & \text{elsewhere.} \end{cases}$$

The corresponding basis functions can be generated using dilation parameter j and translation parameter k as $\{\phi_k^j(x) = 2^{j/2}\phi(2^j x - k)\}_{j,k \in \mathbb{Z}}$, $\{\psi_k^j(x) = 2^{j/2}\psi(2^j x - k)\}_{j,k \in \mathbb{Z}}$ to form an orthonormal subfamily of the Hilbert space $L^2(\mathbb{R})$. Let us choose $i = m + k + 1$, where $m = 2^j$ for $j = 0, 1, \dots, J$ and $k = 0, 1, \dots, m - 1$.

245 Then, for $t \in [0, 1]$, the i^{th} Haar wavelet is defined as:

$$\psi_i(x) = \begin{cases} 1, & \text{for } x \in [\zeta_1(i), \zeta_2(i)), \\ -1, & \text{for } x \in [\zeta_2(i), \zeta_3(i)), \\ 0, & \text{elsewhere,} \end{cases} \quad i = 2, 3, \dots, \quad (3.18)$$

where $\zeta_1(i) = \frac{k}{m}$, $\zeta_2(i) = \frac{k+1/2}{m}$, $\zeta_3(i) = \frac{k+1}{m}$. J is called the maximum level of resolution. Further, the n^{th} , $n \in \mathbb{N}$ integration of the Haar wavelets can be written as:

$$\mathcal{R}_{n,1}(x) = \frac{x^n}{n!}, \quad \text{for all } x \in [0, 1), \quad (3.19)$$

and for $i = 2, 3, \dots$,

$$\mathcal{R}_{n,i}(x) = \frac{1}{n!} \begin{cases} 0, & 0 \leq x < \zeta_1(i), \\ (x - \zeta_1(i))^n, & \zeta_1(i) \leq x < \zeta_2(i), \\ (x - \zeta_1(i))^n - 2(x - \zeta_2(i))^n, & \zeta_2(i) \leq x < \zeta_3(i), \\ (x - \zeta_1(i))^n - 2(x - \zeta_2(i))^n + (x - \zeta_3(i))^n, & \zeta_3(i) \leq x < 1. \end{cases} \quad (3.20)$$

The following lemma shows the upper bounds of the integrands of the Haar wavelets that help to obtain the required error bounds described in Theorem 4.8.

250

Lemma 3.2. (Theorem 1, [38]) The n^{th} ($n \in \mathbb{N}$) integration of the Haar wavelets defined in (3.19) and (3.20) satisfies the following bounds.

$$\begin{cases} |\mathcal{R}_{n,1}(t)| \leq \frac{1}{n!}, & n \geq 1, \\ |\mathcal{R}_{1,i}(t)| \leq \frac{1}{2^{j+1}}, & i \geq 2, \\ |\mathcal{R}_{n,i}(t)| \leq \mathcal{C}(n) \left(\frac{1}{2^{j+1}}\right)^2, & n \geq 2, i \geq 2, \end{cases}$$

where $\mathcal{C}(n) = \frac{8}{3(\lfloor (n+1)/2 \rfloor!)^2}$.

A real-valued function $z(x, y) \in L^2(\bar{\mathcal{G}})$ can be decomposed by using two-dimensional Haar wavelets as:

$$z(x, y) = D_{1,1}\phi(x)\phi(y) + \sum_{i_2=2}^{\infty} D_{1,i_2}\phi(x)\psi_{i_2}(y) + \sum_{i_1=2}^{\infty} D_{i_1,1}\psi_{i_1}(x)\phi(y) + \sum_{i_1=2}^{\infty} \sum_{i_2=2}^{\infty} D_{i_1,i_2}\psi_{i_1}(x)\psi_{i_2}(y).$$

255 Its numerical approximation is given by

$$\begin{aligned} z(x, y) &\approx z_{M_1 M_2}(x, y) := D_{1,1}\phi(x)\phi(y) + \sum_{i_2=2}^{2M_2} D_{1,i_2}\phi(x)\psi_{i_2}(y) + \sum_{i_1=2}^{2M_1} D_{i_1,1}\psi_{i_1}(x)\phi(y) + \sum_{i_1=2}^{2M_1} \sum_{i_2=2}^{2M_2} D_{i_1,i_2}\psi_{i_1}(x)\psi_{i_2}(y) \\ &= \mathbf{H}(x)^T \mathbf{D} \mathbf{H}(y), \end{aligned} \quad (3.21)$$

where $\mathbf{H}(x) = (\phi(x), \psi_2(x), \dots, \psi_{2M_1}(x))^T$, $\mathbf{H}(y) = (\phi(y), \psi_2(y), \dots, \psi_{2M_2}(y))^T$, and \mathbf{D} is the matrix of unknown coefficients of order $(2M_1 \times 2M_2)$, given by

$$\mathbf{D} = \begin{pmatrix} D_{1,1} & D_{1,2} & \cdots & D_{1,2M_2} \\ D_{2,1} & D_{2,2} & \cdots & D_{2,2M_2} \\ \vdots & \vdots & \ddots & \vdots \\ D_{2M_1,1} & D_{2M_1,2} & \cdots & D_{2M_1,2M_2} \end{pmatrix}. \quad (3.22)$$

Here, we take $i_1 = m_1 + k_1 + 1$, with $m_1 = 2^{j_1}$ for $j_1 = 0, 1, \dots, J_1$ and $k_1 = 0, 1, \dots, m_1 - 1$. $i_2 = m_2 + k_2 + 1$, with $m_2 = 2^{j_2}$ for $j_2 = 0, 1, \dots, J_2$ and $k_2 = 0, 1, \dots, m_2 - 1$. J_1 and J_2 represent the maximum level of resolution in the direction of x and y , respectively. Further, $M_1 = 2^{J_1}$, $M_2 = 2^{J_2}$. In order to find the unknown matrix, we use the two-dimensional collocation points $\{(x_{l_1}, y_{l_2})\}_{l_1=1, l_2=1}^{2M_1, 2M_2}$ defined as:

$$x_{l_1} = \frac{l_1 - 1/2}{2M_1}, \quad y_{l_2} = \frac{l_2 - 1/2}{2M_2}, \quad l_1 = 1, 2, \dots, 2M_1, \quad l_2 = 1, 2, \dots, 2M_2. \quad (3.23)$$

Let us assume $\mathcal{U}_{xxyy}^{n+\sigma}(x, y) \in L^2(\bar{\mathcal{G}})$. Then, $\mathcal{U}_{xxyy}^{n+\sigma}(x, y)$ can be approximated as:

$$\mathcal{U}_{xxyy}^{n+\sigma}(x, y) \approx \mathbf{H}(x)^T \mathbf{D} \mathbf{H}(y). \quad (3.24)$$

Integrating (3.24) with respect to y twice and using the boundary conditions given in (3.16), we obtain:

$$\mathcal{U}_{xx}^{n+\sigma}(x, y) \approx \mathbf{H}(x)^T \mathbf{D} (\mathcal{R}_2(y) - y \mathcal{R}_2(1)) + (1 - y) \frac{\partial^2 h_3}{\partial x^2}(x, t_{n+\sigma}) + y \frac{\partial^2 h_4}{\partial x^2}(x, t_{n+\sigma}), \quad (3.25)$$

where $\mathcal{R}_2(y) := (\mathcal{R}_{2,1}(y), \mathcal{R}_{2,2}(y), \dots, \mathcal{R}_{2,2M_2}(y))^T$. Again, integrating (3.24) with respect to x two times and then, using the boundary conditions, we yield

$$\mathcal{U}_{yy}^{n+\sigma}(x, y) \approx (\mathcal{R}_2(x) - x \mathcal{R}_2(1))^T \mathbf{D} \mathbf{H}(y) + (1 - x) \frac{\partial^2 h_1}{\partial y^2}(y, t_{n+\sigma}) + x \frac{\partial^2 h_2}{\partial y^2}(y, t_{n+\sigma}), \quad (3.26)$$

with $\mathcal{R}_2(x) := (\mathcal{R}_{2,1}(x), \mathcal{R}_{2,2}(x), \dots, \mathcal{R}_{2,2M_1}(x))^T$. Further, the integration of (3.25) with respect to x twice,

and the integration of (3.26) with respect to y once yields the following:

$$\begin{aligned}\mathcal{U}_x^{n+\sigma}(x, y) &\approx (\mathcal{R}_1(x) - \mathcal{R}_2(1))^T \mathbf{D}(\mathcal{R}_2(y) - y\mathcal{R}_2(1)) - h_1(y, t_{n+\sigma}) + h_2(y, t_{n+\sigma}) \\ &\quad + (1-y) \left(\frac{\partial h_3}{\partial x}(x, t_{n+\sigma}) - h_3(1, t_{n+\sigma}) + h_3(0, t_{n+\sigma}) \right) \\ &\quad + y \left(\frac{\partial h_4}{\partial x}(x, t_{n+\sigma}) - h_4(1, t_{n+\sigma}) + h_4(0, t_{n+\sigma}) \right),\end{aligned}\tag{3.27}$$

$$\begin{aligned}\mathcal{U}_y^{n+\sigma}(x, y) &\approx (\mathcal{R}_2(x) - x\mathcal{R}_2(1))^T \mathbf{D}(\mathcal{R}_1(y) - \mathcal{R}_2(1)) - h_3(x, t_{n+\sigma}) + h_4(x, t_{n+\sigma}) \\ &\quad + (1-x) \left(\frac{\partial h_1}{\partial y}(y, t_{n+\sigma}) - h_1(1, t_{n+\sigma}) + h_1(0, t_{n+\sigma}) \right) \\ &\quad + x \left(\frac{\partial h_2}{\partial y}(y, t_{n+\sigma}) - h_2(1, t_{n+\sigma}) + h_2(0, t_{n+\sigma}) \right),\end{aligned}\tag{3.28}$$

$$\begin{aligned}\mathcal{U}^{n+\sigma}(x, y) &\approx (\mathcal{R}_2(x) - x\mathcal{R}_2(1))^T \mathbf{D}(\mathcal{R}_2(y) - y\mathcal{R}_2(1)) + (1-x)h_1(y, t_{n+\sigma}) + xh_2(y, t_{n+\sigma}) \\ &\quad + (1-y)(h_3(x, t_{n+\sigma}) - h_3(0, t_{n+\sigma}) - xh_3(1, t_{n+\sigma}) + xh_3(0, t_{n+\sigma})) \\ &\quad + y(h_4(x, t_{n+\sigma}) - h_4(0, t_{n+\sigma}) - xh_4(1, t_{n+\sigma}) + xh_4(0, t_{n+\sigma})),\end{aligned}\tag{3.29}$$

where $\mathcal{R}_1(x) := (\mathcal{R}_{1,1}(x), \mathcal{R}_{1,2}(x), \dots, \mathcal{R}_{1,2M_1}(x))^T$, $\mathcal{R}_1(y) := (\mathcal{R}_{1,1}(y), \mathcal{R}_{1,2}(y), \dots, \mathcal{R}_{1,2M_2}(y))^T$. Now, using Lemma 3.1 in (3.29), we have

$$\begin{aligned}\mathcal{U}^{n+1}(x, y) &\approx \frac{1}{\sigma} \left[(\mathcal{R}_2(x) - x\mathcal{R}_2(1))^T \mathbf{D}(\mathcal{R}_2(y) - y\mathcal{R}_2(1)) + (1-x)h_1(y, t_{n+\sigma}) + xh_2(y, t_{n+\sigma}) \right. \\ &\quad + (1-y)(h_3(x, t_{n+\sigma}) - h_3(0, t_{n+\sigma}) - xh_3(1, t_{n+\sigma}) + xh_3(0, t_{n+\sigma})) \\ &\quad + y(h_4(x, t_{n+\sigma}) - h_4(0, t_{n+\sigma}) - xh_4(1, t_{n+\sigma}) + xh_4(0, t_{n+\sigma})) \left. \right] \\ &\quad - \left(\frac{1-\sigma}{\sigma} \right) \mathcal{U}^n(x, y),\end{aligned}\tag{3.30}$$

270 Substituting (3.25)-(3.30) into (3.16), one can have a linear system at each time level and that can be solved by using the collocation points defined in (3.23). Then, after substituting the wavelet coefficients into (3.30), we obtain the numerical solution of (1.2) at each time level. The algorithm for scientific computing is described in Algorithm 2 in support of the two-dimensional TFIPDEs.

Note 1. *One-dimensional TFIPDE (1.1) can also be solved using the semi-discretization technique described in Section 3.2.1. In this case, we must apply the one-dimensional Haar wavelet approximation to approximate the spatial derivatives.*

4. Stability and convergence analysis

In this section, we present the stability and the convergence analysis of the proposed schemes for solving TFIPDEs of type (1.1) and (1.2). Further investigation shows that the present methods lead to higher-order approximations (see Theorems 4.3 and 4.10) in comparison with the solution obtained by $L1$ discretization

280

Algorithm 2 ALGORITHM FOR THE SOLUTION OF TWO-DIMENSIONAL TFIPDEs

- 1: **Input 1:** α ▷ Order of the fractional operator
 - 2: **Input 2:** N ▷ Number of mesh interval towards time
 - 3: **Input 2:** J_1, J_2 ▷ Maximum level of resolution towards x, y
 - 4: **Input 4:** g, h_1, h_2, h_3, h_4 ▷ Initial and boundary conditions
 - 5: Compute $\sigma = 1 - (\alpha/2)$
 - 6: Compute $\Delta t = T/N$ ▷ Mesh parameters
 - 7: Compute $t_n = n * \Delta t$ for $n = 0, 1, \dots, N$
 - 8: Compute $M_1 = 2^{J_1}, M_2 = 2^{J_2}$
 - 9: Compute $\{(x_{l_1}, y_{l_2})\}_{l_1=1, l_2=1}^{2M_1, 2M_2}$ using (3.23) ▷ The collocation points
 - 10: Compute p_1, p_2, q_1, q_2 and r_1 using collocation points ▷ Coefficient functions
 - 11: Compute \mathcal{K}, f ▷ The given kernel and source term
 - 12: Compute d_0^1 and d_j^{n+1} for $n = 1, 2, \dots, N-1, j = 0, 1, \dots, n-1$ given in (3.1)
 - 13: **for** $n = 0, 1, \dots, N-1$ **do** ▷ Using collocation points and the Kronecker product
 - 14: Compute the operational matrices corresponding to $\mathcal{U}_{xx}^{n+\sigma}, \mathcal{U}_{yy}^{n+\sigma}$ using (3.25), (3.26)
 - 15: Compute the operational matrices corresponding to $\mathcal{U}_x^{n+\sigma}, \mathcal{U}_y^{n+\sigma}$ using (3.27), (3.28)
 - 16: Compute the operational matrices corresponding to $\mathcal{U}^{n+\sigma}, \mathcal{U}^{n+1}$ using (3.29), (3.30)
 - 17: Compute the right-hand side vector by utilizing the source term f
 - 18: Compute the unknown wavelet coefficients $\{D_{i_1, i_2}\}_{i_1=1, i_2=1}^{2M_1, 2M_2}$ by solving the linear system
 - 19: Put the wavelet coefficients in to (3.30) to compute \mathcal{U}^{n+1}
 - 20: **end for**
 - 21: **Output:** Obtained the complete solution \mathcal{U}^{n+1} for $n = 0, 1, \dots, N-1$
-

(see Theorem 4.5 and Remark 4.6). Further, Let $\{\mathcal{U}_m^n\}_{m=0, n=0}^{M, N}$ is the mesh function corresponding to a continuous function $\mathcal{U} : \Omega_{M, N} \rightarrow \mathbb{R}$. Then we define the discrete maximum norm as

$$\|\mathcal{U}\|_\infty := \max_{(x_m, t_n) \in \Omega_{M, N}} |\mathcal{U}(x_m, t_n)| \text{ and } \|\mathcal{U}^n\|_\infty := \max_{0 \leq m \leq M} |\mathcal{U}_m^n|.$$

The stability result will be established later in Theorem 4.2 based on the norm mentioned above. Now, recall the $L2-1_\sigma$ discretization given in (3.1), and rewrite it as:

$${}^{L2-1_\sigma} \mathcal{D}_N^\alpha \mathcal{U}_m^{n+\sigma} = d_n^{n+1} \mathcal{U}_m^{n+1} - d_0^{n+1} \mathcal{U}_m^0 - \sum_{j=1}^n [d_j^{n+1} - d_{j-1}^{n+1}] \mathcal{U}_m^j.$$

285 Therefore, the discrete problem (3.8) can be rewritten as:

$$\left\{ \begin{aligned} & \left[d_n^{n+1} + \frac{2p(x_m)\sigma}{(\Delta x)^2} + r(x_m)\sigma + \frac{\mu\sigma^2\Delta t}{2}\mathcal{K}(x_m, 0) \right] \mathcal{U}_m^{n+1} = d_0^{n+1}\mathcal{U}_m^0 + \sum_{j=1}^n [d_j^{n+1} - d_{j-1}^{n+1}] \mathcal{U}_m^j \\ & \quad + \left[\frac{p(x_m)\sigma}{(\Delta x)^2} + \frac{q(x_m)\sigma}{2\Delta x} \right] \mathcal{U}_{m-1}^{n+1} + \left[\frac{p(x_m)\sigma}{(\Delta x)^2} - \frac{q(x_m)\sigma}{2\Delta x} \right] \mathcal{U}_{m+1}^{n+1} \\ & \quad + \left[\frac{p(x_m)(1-\sigma)}{(\Delta x)^2} + \frac{q(x_m)(1-\sigma)}{2\Delta x} \right] \mathcal{U}_{m-1}^n + \left[\frac{p(x_m)(1-\sigma)}{(\Delta x)^2} - \frac{q(x_m)(1-\sigma)}{2\Delta x} \right] \mathcal{U}_{m+1}^n \\ & \quad - \left[\frac{2p(x_m)(1-\sigma)}{(\Delta x)^2} + r(x_m)(1-\sigma) + \frac{\mu\Delta t}{2}\mathcal{K}(x_m, t_{n+\sigma} - t_n) + \frac{\mu\sigma\Delta t}{2}\mathcal{K}(x_m, t_{n+\sigma} - t_n) \right. \\ & \quad \left. + \frac{\mu\Delta t\sigma(1-\sigma)}{2}\mathcal{K}(x_m, 0) \right] \mathcal{U}_m^n - \frac{\mu\Delta t}{2}\mathcal{K}(x_m, t_{n+\sigma} - t_{n-1})\mathcal{U}_m^{n-1} \\ & \quad - \frac{\mu\Delta t}{2} \sum_{j=0}^{n-2} \left[\mathcal{K}(x_m, t_{n+\sigma} - t_{j+1})\mathcal{U}_m^{j+1} + \mathcal{K}(x_m, t_{n+\sigma} - t_j)\mathcal{U}_m^j \right] + f(x_m, t_{n+\sigma}), \\ & \text{for } m = 1, 2, \dots, M-1; \ n = 0, 1, \dots, N-1, \\ & \mathcal{U}_m^0 = g(x_m) \text{ for } m = 0, 1, \dots, M, \ \mathcal{U}_0^n = h_1(t_n) \text{ and } \mathcal{U}_M^n = h_2(t_n) \text{ for } n = 0, 1, \dots, N. \end{aligned} \right. \quad (4.1)$$

The following lemma provides the truncation error bound that occurs because of the approximation of the fractional operator, which is expressed as follows:

Lemma 4.1. *Let $\alpha \in (0, 1)$ and $\mathcal{U} \in C^3(\bar{\Omega}, \mathbb{R})$. Then, for any $(x_m, t_{n+\sigma}) \in \Omega_{M,N}$, we have*

$$\left| (\partial_t^\alpha - {}^{L2-1}\sigma \mathcal{D}_N^\alpha) \mathcal{U}(x_m, t_{n+\sigma}) \right| \leq C(\Delta t)^{3-\alpha}.$$

Proof. The detailed proof of this technical lemma is available in [31]. □

290 We now establish the stability estimate of the proposed numerical approximation in favor of the one-dimensional TFIPDEs (1.1), which will be used later in Theorem 4.3 to show the main convergence result.

Theorem 4.2. *The solution of the discrete problem (3.8) satisfies the following inequality*

$$\|\mathcal{U}^{n+1}\|_\infty \leq \|\mathcal{U}^0\|_\infty + 2T^\alpha \Gamma(1-\alpha) \max_{0 \leq n \leq N-1} \|f^{n+\sigma}\|_\infty, \quad n = 0, 1, \dots, N-1,$$

provided $d_n^{n+1} > d_{n-1}^{n+1} > \dots > d_0^{n+1} \geq \mathcal{C} > 0$, for $n = 0, 1, \dots, N-1$ with $\mathcal{C} = \frac{1}{2T^\alpha \Gamma(1-\alpha)}$.

Proof. For any fixed $n \in \{0, 1, \dots, N-1\}$, choose an m^* such that $\|\mathcal{U}^{n+1}\|_\infty = |\mathcal{U}_{m^*}^{n+1}|$. From (4.1), we have

$$\begin{aligned} & \left[d_n^{n+1} + \frac{2p(x_{m^*})\sigma}{(\Delta x)^2} + r(x_{m^*})\sigma + \frac{\mu\sigma^2\Delta t}{2}\mathcal{K}(x_{m^*}, 0) \right] \mathcal{U}_{m^*}^{n+1} = d_0^{n+1}\mathcal{U}_{m^*}^0 + \sum_{j=1}^n [d_j^{n+1} - d_{j-1}^{n+1}] \mathcal{U}_{m^*}^j \\ & \quad + \left[\frac{p(x_{m^*})\sigma}{(\Delta x)^2} + \frac{q(x_{m^*})\sigma}{2\Delta x} \right] \mathcal{U}_{m^*-1}^{n+1} + \left[\frac{p(x_{m^*})\sigma}{(\Delta x)^2} - \frac{q(x_{m^*})\sigma}{2\Delta x} \right] \mathcal{U}_{m^*+1}^{n+1} \\ & \quad + \left[\frac{p(x_{m^*})(1-\sigma)}{(\Delta x)^2} + \frac{q(x_{m^*})(1-\sigma)}{2\Delta x} \right] \mathcal{U}_{m^*-1}^n + \left[\frac{p(x_{m^*})(1-\sigma)}{(\Delta x)^2} - \frac{q(x_{m^*})(1-\sigma)}{2\Delta x} \right] \mathcal{U}_{m^*+1}^n \\ & \quad - \left[\frac{2p(x_{m^*})(1-\sigma)}{(\Delta x)^2} + r(x_{m^*})(1-\sigma) + \frac{\mu\Delta t}{2}\mathcal{K}(x_{m^*}, t_{n+\sigma} - t_n) + \frac{\mu\sigma\Delta t}{2}\mathcal{K}(x_{m^*}, t_{n+\sigma} - t_n) \right. \\ & \quad \left. + \frac{\mu\Delta t\sigma(1-\sigma)}{2}\mathcal{K}(x_{m^*}, 0) \right] \mathcal{U}_{m^*}^n - \frac{\mu\Delta t}{2}\mathcal{K}(x_{m^*}, t_{n+\sigma} - t_{n-1})\mathcal{U}_{m^*}^{n-1} \\ & \quad - \frac{\mu\Delta t}{2} \sum_{j=0}^{n-2} \left[\mathcal{K}(x_{m^*}, t_{n+\sigma} - t_{j+1})\mathcal{U}_{m^*}^{j+1} + \mathcal{K}(x_{m^*}, t_{n+\sigma} - t_j)\mathcal{U}_{m^*}^j \right] + f(x_{m^*}, t_{n+\sigma}). \end{aligned}$$

295 Keeping in mind that $\sigma \in (0, 1)$, $r \geq 0$, and the kernel $\mathcal{K} \geq 0$ together with the condition defined in (3.11) and the choice of m^* yields

$$\begin{aligned} \left[d_n^{n+1} + \frac{2p(x_{m^*})\sigma}{(\Delta x)^2} \right] \|\mathcal{U}^{n+1}\|_\infty &\leq d_0^{n+1} \|\mathcal{U}^0\|_\infty + \sum_{j=1}^n [d_j^{n+1} - d_{j-1}^{n+1}] \|\mathcal{U}^j\|_\infty \\ &\quad + \left[\frac{p(x_{m^*})\sigma}{(\Delta x)^2} + \frac{q(x_{m^*})\sigma}{2\Delta x} \right] \|\mathcal{U}^{n+1}\|_\infty + \left[\frac{p(x_{m^*})\sigma}{(\Delta x)^2} - \frac{q(x_{m^*})\sigma}{2\Delta x} \right] \|\mathcal{U}^{n+1}\|_\infty \\ &\quad + \left[\frac{p(x_{m^*})(1-\sigma)}{(\Delta x)^2} + \frac{q(x_{m^*})(1-\sigma)}{2\Delta x} \right] \|\mathcal{U}^n\|_\infty + \left[\frac{p(x_{m^*})(1-\sigma)}{(\Delta x)^2} \right. \\ &\quad \left. - \frac{q(x_{m^*})(1-\sigma)}{2\Delta x} \right] \|\mathcal{U}^n\|_\infty - \left[\frac{2p(x_{m^*})(1-\sigma)}{(\Delta x)^2} \right] \|\mathcal{U}^n\|_\infty + \|f^{n+\sigma}\|_\infty. \end{aligned}$$

The given condition $d_n^{n+1} > d_{n-1}^{n+1} > \dots > d_0^{n+1} \geq \mathcal{C} > 0$ enables us to have

$$\begin{aligned} d_n^{n+1} \|\mathcal{U}^{n+1}\|_\infty &\leq \sum_{j=1}^n [d_j^{n+1} - d_{j-1}^{n+1}] \|\mathcal{U}^j\|_\infty + d_0^{n+1} \left[\|\mathcal{U}^0\|_\infty + 2T^\alpha \Gamma(1-\alpha) \|f^{n+\sigma}\|_\infty \right] \\ &\leq \sum_{j=1}^n [d_j^{n+1} - d_{j-1}^{n+1}] \|\mathcal{U}^j\|_\infty + d_0^{n+1} \left[\|\mathcal{U}^0\|_\infty + 2T^\alpha \Gamma(1-\alpha) \max_{0 \leq n \leq N-1} \|f^{n+\sigma}\|_\infty \right]. \end{aligned} \quad (4.2)$$

Let us take $\mathcal{D} = \|\mathcal{U}^0\|_\infty + 2T^\alpha \Gamma(1-\alpha) \max_{0 \leq n \leq N-1} \|f^{n+\sigma}\|_\infty$. We now use mathematical induction to prove this theorem. For $n = 0$, the theorem is automatically satisfied from (4.2). Let us assume that the inequality

300 holds true for $n = 1, 2, \dots, k-1$, i.e. $\|\mathcal{U}^{n+1}\|_\infty \leq \mathcal{D}$, $n = 1, \dots, k-1$. Now, from (4.2), we have

$$\begin{aligned} d_k^{k+1} \|\mathcal{U}^{k+1}\|_\infty &\leq \sum_{j=1}^k (d_j^{k+1} - d_{j-1}^{k+1}) \|\mathcal{U}^j\|_\infty + d_0^{k+1} \mathcal{D} \leq \sum_{j=1}^k (d_j^{k+1} - d_{j-1}^{k+1}) \mathcal{D} + d_0^{k+1} \mathcal{D} = d_k^{k+1} \mathcal{D} \\ \Rightarrow \|\mathcal{U}^{k+1}\|_\infty &\leq \mathcal{D} = \|\mathcal{U}^0\|_\infty + 2T^\alpha \Gamma(1-\alpha) \max_{0 \leq n \leq N-1} \|f^{n+\sigma}\|_\infty. \end{aligned}$$

Hence, the theorem is proved. \square

The error equation can be obtained by subtracting (3.8) from (3.6) as follows:

$$\left\{ \begin{array}{l} {}^{L2-1_\sigma} \mathcal{D}_N^\alpha e_m^{n+\sigma} - p(x_m) \delta_{\Delta x, \Delta t}^2 e_m^{n+\sigma} + q(x_m) D_{\Delta x, \Delta t}^0 e_m^{n+\sigma} + r(x_m) e_m^{n+\sigma} + \mu \mathcal{J}_N e_m^{n+\sigma} = {}^{L2-1_\sigma} \mathcal{R}_m^{n+\sigma}, \\ \text{for } m = 1, 2, \dots, M-1; \ n = 0, 1, \dots, N-1, \\ e_m^0 = 0 \text{ for } m = 0, 1, \dots, M, \\ e_0^n = e_M^n = 0 \text{ for } n = 0, 1, \dots, N, \end{array} \right. \quad (4.3)$$

where ${}^{L2-1_\sigma} \mathcal{R}_m^{n+\sigma}$ is the remainder term defined in (3.7), and $e_m^{n+\sigma} = \mathcal{U}(x_m, t_{n+\sigma}) - \mathcal{U}_m^{n+\sigma}$.

4.1. Convergence based on $L2-1_\sigma$ scheme

305 In this section, we present the main convergence result of the proposed scheme for the model (1.1). The effect of each term (in particular, the fractional operator, integral term, and spatial derivatives) on the error estimate is being analyzed.

Theorem 4.3. If (1.1) has a solution $\mathcal{U} \in C_{x,t}^{4,3}(\bar{\Omega}, \mathbb{R})$ and let $\{\mathcal{U}(x_m, t_n)\}_{m=0, n=0}^{M, N}$ and $\{\mathcal{U}_m^n\}_{m=0, n=0}^{M, N}$ be the exact and numerical solutions of (1.1) by using the discrete scheme (3.8), respectively. Then, one has the following error bound:

$$\|e\|_\infty \leq C[(\Delta t)^{3-\alpha} + (\Delta t)^2 + (\Delta x)^2].$$

Proof. Theorem 4.2 implies that the solution of the discrete problem (4.3) satisfies the following bound for $n = 0, 1, \dots, N-1$.

$$\begin{aligned} \|e^{n+1}\|_\infty &\leq \|e^0\|_\infty + 2T^\alpha \Gamma(1-\alpha) \max_{0 \leq n \leq N-1} \|L^{2-1_\sigma} \mathcal{R}^{n+\sigma}\|_\infty \\ \Rightarrow \|e^{n+1}\|_\infty &\leq 2T^\alpha \Gamma(1-\alpha) \max_{0 \leq n \leq N-1} \|L^{2-1_\sigma} \mathcal{R}^{n+\sigma}\|_\infty \\ &\leq C \max_{0 \leq n \leq N-1} \left\| \left(\partial_t^\alpha - L^{2-1_\sigma} \mathcal{D}_N^\alpha \right) \mathcal{U}^{n+\sigma} \right\|_\infty + O((\Delta t)^2 + (\Delta x)^2). \end{aligned}$$

Now, using Lemma 4.1, we get

$$\|e\|_\infty = \max_{0 \leq n \leq N-1} \|e^{n+1}\|_\infty \leq C[(\Delta t)^{3-\alpha} + (\Delta t)^2 + (\Delta x)^2].$$

□

Note 2. For L^{2-1_σ} scheme, it can be observed that the truncation error bound $O((\Delta t)^{3-\alpha})$ corresponding to the fractional operator is dominated by the truncation error bound $O((\Delta t)^2)$. Hence the proposed scheme provides an overall second-order convergence for any value of $\alpha \in (0, 1)$ (see Tables 1, 2, 3, 4 of Section 5).

The following lemma reveals the truncation error bound for approximating the fractional operator based on the L^1 scheme that will be utilized later in Theorem 4.5 to estimate the convergence result.

Lemma 4.4. If $\mathcal{U} \in C^2(\bar{\Omega}, \mathbb{R})$, the truncation error corresponding to the L^1 scheme satisfies the following bound:

$$\left| \left(\partial_t^\alpha - L^1 \mathcal{D}_N^\alpha \right) \mathcal{U}(x_m, t_n) \right| \leq C(\Delta t)^{2-\alpha}, \text{ for } (x_m, t_n) \in \Omega_{M,N}. \quad (4.4)$$

Proof. A similar kind of proof is available in [20, 39].

□

4.2. Convergence based on L^1 scheme

Theorem 4.5. If (1.1) has a solution in $C_{x,t}^{4,2}(\bar{\Omega}, \mathbb{R})$, then, the solution of the discrete problem (3.12) converges to the exact solution of (1.1) with an error \tilde{e}_m^n , $m = 0, 1, \dots, M$; $n = 0, 1, \dots, N$, satisfying the following bound with respect to the L_∞ -norm.

$$\|\tilde{e}\|_\infty \leq C[(\Delta t)^{2-\alpha} + (\Delta t)^2 + (\Delta x)^2].$$

Proof. The proof of this lemma is available in [40] for a time-fractional diffusion equation and it can be extended by introducing the truncation error bound $O((\Delta t)^2)$, occurred due to the presence of the Volterra integral operator.

□

Note 3. In the case of L1 scheme, the truncation error bounds corresponding to the integral operator as well as the spatial derivative are dominated by the truncation error bound $O((\Delta t)^{2-\alpha})$ occurred due to the discretization of the fractional operator, where $\alpha \in (0, 1)$. Hence, the L1 scheme provides a $2 - \alpha$ rate of convergence globally. Additionally, see Tables 2, 3, 4 at Section 5.

Remark 4.6. For α tends to 1, it can be observed that the L1 scheme gives an almost 1st order convergence rate, whereas the L2-1 $_{\sigma}$ scheme produces 2nd order accuracy for the given problem (1.1) (see also Tables 2, 3, and 4 of Section 5).

4.3. Convergence based on two-dimensional Haar wavelets

In this section, our objective is to demonstrate the convergence of the numerical approximation based on two-dimensional Haar wavelets in the context of two-dimensional TFIPDEs depicted in (1.2) by using their orthogonality property given by

$$\int_0^1 \psi_{i_1}(x) \psi_{i'_1}(x) dx = \begin{cases} \frac{1}{2^{j_1}}, & \text{if } i_1 = i'_1, \\ 0, & \text{if } i_1 \neq i'_1 \end{cases}, \quad \int_0^1 \psi_{i_2}(y) \psi_{i'_2}(y) dy = \begin{cases} \frac{1}{2^{j_2}}, & \text{if } i_2 = i'_2, \\ 0, & \text{if } i_2 \neq i'_2 \end{cases}. \quad (4.5)$$

Keeping in mind the wavelet-based numerical approximation (3.21), the coefficients given in (3.22) can be determined by using the orthogonality properties (4.5), as:

$$D_{i_1, i_2} := \int_0^1 \int_0^1 z(x, y) \psi_{i_1}(x) \psi_{i_2}(y) dx dy$$

with $\psi_{i_1}(x) = \phi(x)$, $\psi_{i_2}(y) = \phi(y)$ when $i_1 = 1$, $i_2 = 1$, respectively. The following lemma demonstrates the bounds for the wavelet coefficients that will be used later in Theorem 4.8 to obtain the error bounds for the wavelet-based numerical solutions.

Lemma 4.7. Let $z(x, y) \in L^2([0, 1] \times [0, 1])$ be continuous, and if $z_{M_1 M_2}(x, y)$ is the numerical approximation to $z(x, y)$ based on the two-dimensional Haar wavelets given in (3.21), then the wavelet coefficients $\{D_{i_1, i_2}\}_{i_1=1, i_2=1}^{\infty, \infty}$ satisfy the following bounds.

$$\begin{cases} |D_{1,1}| \leq \mathcal{M}, \\ |D_{1, i_2}| \leq \frac{\mathcal{M}}{2^{j_2+1}}, & \text{for } i_2 \geq 2, \\ |D_{i_1, 1}| \leq \frac{\mathcal{M}}{2^{j_1+1}}, & \text{for } i_1 \geq 2, \\ |D_{i_1, i_2}| \leq \frac{\mathcal{M}}{(2^{j_1+1})(2^{j_2+1})}, & \text{for } i_1 \geq 2, i_2 \geq 2, \end{cases}$$

provided $|z|, |z_x|, |z_y|, |z_{xy}| \leq \mathcal{M}$, for all $(x, y) \in \bar{\mathcal{G}}$. \mathcal{M} is some positive constant.

Proof. Applying the mean value theorem for integrals, we have

$$\begin{aligned} |D_{1,1}| &= \left| \int_0^1 \int_0^1 z(x, y) \phi(x) \phi(y) dx dy \right| = \left| \int_0^1 \int_0^1 z(x, y) dx dy \right| = \left| \int_0^1 z(\rho_1, y) dy \right| \\ &= \left| z(\rho_1, \rho_2) \int_0^1 dy \right| = |z(\rho_1, \rho_2)| \leq \mathcal{M}, \text{ for some } \rho_1, \rho_2 \in (0, 1). \end{aligned}$$

For $i_2 \geq 2$, following (3.18), and the mean value theorem for integrals yields

$$\begin{aligned} D_{1,i_2} &= \int_0^1 \int_0^1 z(x,y) \phi(x) \psi_{i_2}(y) dx dy = \int_0^1 \int_0^1 z(x,y) \psi_{i_2}(y) dx dy = \int_0^1 z(\rho_3, y) \psi_{i_2}(y) dy \\ &= \int_{k_2/2^{j_2}}^{(k_2+\frac{1}{2})/2^{j_2}} z(\rho_3, y) dy - \int_{(k_2+\frac{1}{2})/2^{j_2}}^{(k_2+1)/2^{j_2}} z(\rho_3, y) dy = \frac{1}{2^{j_2+1}} (z(\rho_3, \rho_4) - z(\rho_3, \rho_5)) \\ &= \frac{1}{2^{j_2+1}} (\rho_4 - \rho_5) \frac{\partial z}{\partial y} \Big|_{x=\rho_3, y=\rho_6}, \end{aligned}$$

350 for some $\rho_3 \in (0, 1)$, $\rho_4 \in \left(\frac{k_2}{2^{j_2}}, \frac{k_2+\frac{1}{2}}{2^{j_2}}\right)$, $\rho_5 \in \left(\frac{k_2+\frac{1}{2}}{2^{j_2}}, \frac{k_2+1}{2^{j_2}}\right)$, and $\rho_6 \in (\min\{\rho_4, \rho_5\}, \max\{\rho_4, \rho_5\})$.

Hence,

$$\left| D_{1,i_2} \right| = \left| \frac{1}{2^{j_2+1}} (\rho_4 - \rho_5) \frac{\partial z}{\partial y} \Big|_{x=\rho_3, y=\rho_6} \right| \leq \frac{1}{2^{j_2+1}} |\rho_4 - \rho_5| \left| \frac{\partial z}{\partial y} \Big|_{x=\rho_3, y=\rho_6} \right| \leq \frac{\mathcal{M}}{2^{j_2+1}}.$$

Using similar arguments, one can prove $\left| D_{i_1,1} \right| \leq \frac{\mathcal{M}}{2^{j_1+1}}$, for $i_1 \geq 2$. Finally, for $i_1 \geq 2$, $i_2 \geq 2$, we have

$$\begin{aligned} D_{i_1,i_2} &= \int_0^1 \int_0^1 z(x,y) \psi_{i_1}(x) \psi_{i_2}(y) dx dy \\ &= \int_0^1 \left(\int_{k_1/2^{j_1}}^{(k_1+\frac{1}{2})/2^{j_1}} z(x,y) dx - \int_{(k_1+\frac{1}{2})/2^{j_1}}^{(k_1+1)/2^{j_1}} z(x,y) dx \right) \psi_{i_2}(y) dy \\ &= \frac{1}{2^{j_1+1}} \int_0^1 (z(\rho_7, y) - z(\rho_8, y)) \psi_{i_2}(y) dy = \frac{(\rho_7 - \rho_8)}{2^{j_1+1}} \int_0^1 \frac{\partial z}{\partial x}(\rho_9, y) \psi_{i_2}(y) dy \\ &= \frac{(\rho_7 - \rho_8)}{2^{j_1+1}} \left(\int_{k_2/2^{j_2}}^{(k_2+\frac{1}{2})/2^{j_2}} \frac{\partial z}{\partial x}(\rho_9, y) dy - \int_{(k_2+\frac{1}{2})/2^{j_2}}^{(k_2+1)/2^{j_2}} \frac{\partial z}{\partial x}(\rho_9, y) dy \right) \\ &= \frac{(\rho_7 - \rho_8)}{(2^{j_1+1})(2^{j_2+1})} \left(\frac{\partial z}{\partial x}(\rho_9, \rho_{10}) - \frac{\partial z}{\partial x}(\rho_9, \rho_{11}) \right) = \frac{(\rho_7 - \rho_8)(\rho_{10} - \rho_{11})}{(2^{j_1+1})(2^{j_2+1})} \frac{\partial^2 z}{\partial y \partial x} \Big|_{x=\rho_9, y=\rho_{12}}, \end{aligned}$$

for some $\rho_7 \in \left(\frac{k_1}{2^{j_1}}, \frac{k_1+\frac{1}{2}}{2^{j_1}}\right)$, $\rho_8 \in \left(\frac{k_1+\frac{1}{2}}{2^{j_1}}, \frac{k_1+1}{2^{j_1}}\right)$, $\rho_9 \in (\min\{\rho_7, \rho_8\}, \max\{\rho_7, \rho_8\})$, $\rho_{10} \in \left(\frac{k_2}{2^{j_2}}, \frac{k_2+\frac{1}{2}}{2^{j_2}}\right)$, $\rho_{11} \in \left(\frac{k_2+\frac{1}{2}}{2^{j_2}}, \frac{k_2+1}{2^{j_2}}\right)$, and $\rho_{12} \in (\min\{\rho_{10}, \rho_{11}\}, \max\{\rho_{10}, \rho_{11}\})$. Taking the modulus on both sides of the

355 above equation, we obtain:

$$\begin{aligned} \left| D_{i_1,i_2} \right| &= \left| \frac{(\rho_7 - \rho_8)(\rho_{10} - \rho_{11})}{(2^{j_1+1})(2^{j_2+1})} \frac{\partial^2 z}{\partial y \partial x} \Big|_{x=\rho_9, y=\rho_{12}} \right| \leq \frac{|\rho_7 - \rho_8| |\rho_{10} - \rho_{11}|}{(2^{j_1+1})(2^{j_2+1})} \left| \frac{\partial^2 z}{\partial y \partial x} \Big|_{x=\rho_9, y=\rho_{12}} \right| \\ &\leq \frac{\mathcal{M}}{(2^{j_1+1})(2^{j_2+1})}. \end{aligned}$$

This completes the proof. \square

As described in Section 3.2.2, if $\mathcal{Q}(x, y) = \mathcal{U}_{xxyy}^{n+\sigma}(x, y) \in L^2(\bar{\mathcal{G}})$, then the Haar wavelet solution at each

time level t_{n+1} , $n = 0, 1, \dots, N-1$, can be expressed as:

$$\begin{aligned}
\mathcal{U}^{n+1}(x, y) \approx & \frac{1}{\sigma} \left[D_{1,1}(\mathcal{R}_{2,1}(x) - x\mathcal{R}_{2,1}(1))(\mathcal{R}_{2,1}(y) - y\mathcal{R}_{2,1}(1)) \right. \\
& + \sum_{i_2=2}^{\infty} D_{1,i_2}(\mathcal{R}_{2,1}(x) - x\mathcal{R}_{2,1}(1))(\mathcal{R}_{2,i_2}(y) - y\mathcal{R}_{2,i_2}(1)) \\
& + \sum_{i_1=2}^{\infty} D_{i_1,1}(\mathcal{R}_{2,i_1}(x) - x\mathcal{R}_{2,i_1}(1))(\mathcal{R}_{2,1}(y) - y\mathcal{R}_{2,1}(1)) \\
& + \left. \sum_{i_1=2}^{\infty} \sum_{i_2=2}^{\infty} D_{i_1,i_2}(\mathcal{R}_{2,i_1}(x) - x\mathcal{R}_{2,i_1}(1))(\mathcal{R}_{2,i_2}(y) - y\mathcal{R}_{2,i_2}(1)) \right] \\
& + \frac{1}{\sigma} \left[(1-x)h_1(y, t_{n+\sigma}) + xh_2(y, t_{n+\sigma}) + (1-y)(h_3(x, t_{n+\sigma}) \right. \\
& - h_3(0, t_{n+\sigma}) - xh_3(1, t_{n+\sigma}) + xh_3(0, t_{n+\sigma})) + y(h_4(x, t_{n+\sigma}) \\
& - h_4(0, t_{n+\sigma}) - xh_4(1, t_{n+\sigma}) + xh_4(0, t_{n+\sigma})) \left. \right] - \left(\frac{1-\sigma}{\sigma} \right) \mathcal{U}^n(x, y), \tag{4.6}
\end{aligned}$$

and its numerical approximation is given by

$$\begin{aligned}
\mathcal{U}_{M_1 M_2}^{n+1}(x, y) \approx & \frac{1}{\sigma} \left[D_{1,1}(\mathcal{R}_{2,1}(x) - x\mathcal{R}_{2,1}(1))(\mathcal{R}_{2,1}(y) - y\mathcal{R}_{2,1}(1)) \right. \\
& + \sum_{i_2=2}^{2M_2} D_{1,i_2}(\mathcal{R}_{2,1}(x) - x\mathcal{R}_{2,1}(1))(\mathcal{R}_{2,i_2}(y) - y\mathcal{R}_{2,i_2}(1)) \\
& + \sum_{i_1=2}^{2M_1} D_{i_1,1}(\mathcal{R}_{2,i_1}(x) - x\mathcal{R}_{2,i_1}(1))(\mathcal{R}_{2,1}(y) - y\mathcal{R}_{2,1}(1)) \\
& + \left. \sum_{i_1=2}^{2M_1} \sum_{i_2=2}^{2M_2} D_{i_1,i_2}(\mathcal{R}_{2,i_1}(x) - x\mathcal{R}_{2,i_1}(1))(\mathcal{R}_{2,i_2}(y) - y\mathcal{R}_{2,i_2}(1)) \right] \\
& + \frac{1}{\sigma} \left[(1-x)h_1(y, t_{n+\sigma}) + xh_2(y, t_{n+\sigma}) + (1-y)(h_3(x, t_{n+\sigma}) \right. \\
& - h_3(0, t_{n+\sigma}) - xh_3(1, t_{n+\sigma}) + xh_3(0, t_{n+\sigma})) + y(h_4(x, t_{n+\sigma}) \\
& - h_4(0, t_{n+\sigma}) - xh_4(1, t_{n+\sigma}) + xh_4(0, t_{n+\sigma})) \left. \right] - \left(\frac{1-\sigma}{\sigma} \right) \mathcal{U}^n(x, y), \tag{4.7}
\end{aligned}$$

360 The error and its L^2 -norm can be defined as:

$$\left\| \mathcal{U}^{n+1}(x, y) - \mathcal{U}_{M_1 M_2}^{n+1}(x, y) \right\|_{L^2} = \left\{ \int_0^1 \int_0^1 |\mathcal{U}^{n+1}(x, y) - \mathcal{U}_{M_1 M_2}^{n+1}(x, y)|^2 dx dy \right\}^{1/2}.$$

The following theorem describes the error bound for the wavelet-based numerical approximation at each time level t_{n+1} , $n = 0, 1, \dots, N-1$, based on L^2 -norm.

Theorem 4.8. Assume that $\mathcal{Q}(x, y) \in L^2(\bar{\mathcal{G}})$ be continuous such that $|\mathcal{Q}|$, $|\mathcal{Q}_x|$, $|\mathcal{Q}_y|$, $|\mathcal{Q}_{xy}| \leq \widetilde{\mathcal{M}}$, the numerical solution (4.7) obtained by the two-dimensional Haar wavelets converges to the exact solution (4.6).

365 Furthermore, the L^2 -norm of the error satisfies the following bound:

$$\left\| \mathcal{U}^{n+1}(x, y) - \mathcal{U}_{M_1 M_2}^{n+1}(x, y) \right\|_{L^2} \leq C \widehat{M}^{-3},$$

where $\widehat{M} = \min\{M_1, M_2\}$ with $M_1 = 2^{J_1}$, $M_2 = 2^{J_2}$; J_1, J_2 are the maximum level of resolutions towards x and y direction, respectively. More precisely, $\left| \mathcal{U}^{n+1}(x, y) - \mathcal{U}_{M_1 M_2}^{n+1}(x, y) \right| \rightarrow 0$ as $\widehat{M} \rightarrow \infty$.

Proof.

$$\begin{aligned} \left\| \mathcal{U}^{n+1}(x, y) - \mathcal{U}_{M_1 M_2}^{n+1}(x, y) \right\|_{L^2}^2 &= \int_0^1 \int_0^1 \left| \mathcal{U}^{n+1}(x, y) - \mathcal{U}_{M_1 M_2}^{n+1}(x, y) \right|^2 dx dy \\ &\leq \mathcal{I}_1 + \mathcal{I}_2 + \mathcal{I}_3 + \mathcal{I}_4 + \mathcal{I}_5 + \mathcal{I}_6, \end{aligned} \quad (4.8)$$

where

$$\begin{aligned} \mathcal{I}_1 &= \sum_{i_2=2M_2+1}^{\infty} \sum_{i'_2=2M_2+1}^{\infty} |D_{1,i_2}| |D_{1,i'_2}| \int_0^1 |\mathcal{R}_{2,1}(x) - x\mathcal{R}_{2,1}(1)|^2 dx \int_0^1 |\mathcal{R}_{2,i_2}(y) - y\mathcal{R}_{2,i_2}(1)| |\mathcal{R}_{2,i'_2}(y) - y\mathcal{R}_{2,i'_2}(1)| dy, \\ \mathcal{I}_2 &= \sum_{i_1=2M_1+1}^{\infty} \sum_{i'_1=2M_1+1}^{\infty} |D_{i_1,1}| |D_{i'_1,1}| \int_0^1 |\mathcal{R}_{2,i_1}(x) - x\mathcal{R}_{2,i_1}(1)| |\mathcal{R}_{2,i'_1}(x) - x\mathcal{R}_{2,i'_1}(1)| dx \int_0^1 |\mathcal{R}_{2,1}(y) - y\mathcal{R}_{2,1}(1)|^2 dy, \\ \mathcal{I}_3 &= \sum_{i_1=2M_1+1}^{\infty} \sum_{i_2=2M_2+1}^{\infty} \sum_{i'_1=2M_1+1}^{\infty} \sum_{i'_2=2M_2+1}^{\infty} |D_{i_1,i_2}| |D_{i'_1,i'_2}| \int_0^1 |\mathcal{R}_{2,i_1}(x) - x\mathcal{R}_{2,i_1}(1)| |\mathcal{R}_{2,i'_1}(x) - x\mathcal{R}_{2,i'_1}(1)| dx \\ &\quad \times \int_0^1 |\mathcal{R}_{2,i_2}(y) - y\mathcal{R}_{2,i_2}(1)| |\mathcal{R}_{2,i'_2}(y) - y\mathcal{R}_{2,i'_2}(1)| dy, \\ \mathcal{I}_4 &= 2 \sum_{i_2=2M_2+1}^{\infty} \sum_{i'_1=2M_1+1}^{\infty} |D_{1,i_2}| |D_{i'_1,1}| \int_0^1 |\mathcal{R}_{2,1}(x) - x\mathcal{R}_{2,1}(1)| |\mathcal{R}_{2,i'_1}(x) - x\mathcal{R}_{2,i'_1}(1)| dx \\ &\quad \times \int_0^1 |\mathcal{R}_{2,i_2}(y) - y\mathcal{R}_{2,i_2}(1)| |\mathcal{R}_{2,1}(y) - y\mathcal{R}_{2,1}(1)| dy, \\ \mathcal{I}_5 &= 2 \sum_{i_2=2M_2+1}^{\infty} \sum_{i'_1=2M_1+1}^{\infty} \sum_{i'_2=2M_2+1}^{\infty} |D_{1,i_2}| |D_{i'_1,i'_2}| \int_0^1 |\mathcal{R}_{2,1}(x) - x\mathcal{R}_{2,1}(1)| |\mathcal{R}_{2,i'_1}(x) - x\mathcal{R}_{2,i'_1}(1)| dx \\ &\quad \times \int_0^1 |\mathcal{R}_{2,i_2}(y) - y\mathcal{R}_{2,i_2}(1)| |\mathcal{R}_{2,i'_2}(y) - y\mathcal{R}_{2,i'_2}(1)| dy, \\ \mathcal{I}_6 &= 2 \sum_{i_1=2M_1+1}^{\infty} \sum_{i'_1=2M_1+1}^{\infty} \sum_{i'_2=2M_2+1}^{\infty} |D_{i_1,1}| |D_{i'_1,i'_2}| \int_0^1 |\mathcal{R}_{2,i_1}(x) - x\mathcal{R}_{2,i_1}(1)| |\mathcal{R}_{2,i'_1}(x) - x\mathcal{R}_{2,i'_1}(1)| dx \\ &\quad \times \int_0^1 |\mathcal{R}_{2,1}(y) - y\mathcal{R}_{2,1}(1)| |\mathcal{R}_{2,i'_2}(y) - y\mathcal{R}_{2,i'_2}(1)| dy, \end{aligned}$$

Applying Lemma 3.2 and Lemma 4.7, one has

$$\begin{aligned} \mathcal{I}_1 &\leq \sum_{i_2=2M_2+1}^{\infty} \sum_{i'_2=2M_2+1}^{\infty} \frac{\widetilde{\mathcal{M}}^2}{2^{j_2+1} 2^{j'_2+1}} \left[\int_0^1 |\mathcal{R}_{2,1}(x)|^2 dx + \int_0^1 x^2 |\mathcal{R}_{2,1}(1)|^2 dx \right. \\ &\quad \left. + \int_0^1 2|x| |\mathcal{R}_{2,1}(x)| |\mathcal{R}_{2,1}(1)| dx \right] \left[\int_0^1 |\mathcal{R}_{2,i_2}(y)| |\mathcal{R}_{2,i'_2}(y)| dy + \int_0^1 |y| |\mathcal{R}_{2,i_2}(y)| |\mathcal{R}_{2,i'_2}(1)| dy \right. \\ &\quad \left. + \int_0^1 |y| |\mathcal{R}_{2,i_2}(1)| |\mathcal{R}_{2,i'_2}(y)| dy + \int_0^1 y^2 |\mathcal{R}_{2,i_2}(1)| |\mathcal{R}_{2,i'_2}(1)| dy \right] \\ &\leq \sum_{j_2=J_2+1}^{\infty} \sum_{j'_2=J_2+1}^{\infty} \frac{\widetilde{\mathcal{M}}^2}{2^{j_2+1} 2^{j'_2+1}} \left[\frac{1}{(2!)^2} + \frac{1}{3(2!)^2} + \frac{1}{(2!)^2} \right] \left[\frac{[\mathcal{C}(2)]^2}{(2^{j_2+1})^2 (2^{j'_2+1})^2} + \frac{[\mathcal{C}(2)]^2}{(2^{j_2+1})^2 (2^{j'_2+1})^2} + \frac{[\mathcal{C}(2)]^2}{3(2^{j_2+1})^2 (2^{j'_2+1})^2} \right] \\ &= \frac{49 \cdot \widetilde{\mathcal{M}}^2 [\mathcal{C}(2)]^2}{3 \cdot 3 \cdot (2!)^2} \sum_{j_2=J_2+1}^{\infty} \frac{1}{(2^{j_2+1})^3} \sum_{j'_2=J_2+1}^{\infty} \frac{1}{(2^{j'_2+1})^3} = \frac{49 \cdot \widetilde{\mathcal{M}}^2 [\mathcal{C}(2)]^2}{3 \cdot 3 \cdot (2!)^2 \cdot 8 \cdot 8} \sum_{j_2=J_2+1}^{\infty} \frac{1}{8^{j_2}} \sum_{j'_2=J_2+1}^{\infty} \frac{1}{8^{j'_2}} \\ &= \frac{49 \cdot \widetilde{\mathcal{M}}^2 [\mathcal{C}(2)]^2}{3 \cdot 3 \cdot (2!)^2 \cdot 8 \cdot 8 \cdot 8^{J_2+1} \cdot 8^{J_2+1}} \sum_{j_2=0}^{\infty} \frac{1}{8^{j_2}} \sum_{j'_2=0}^{\infty} \frac{1}{8^{j'_2}} = \frac{\widetilde{\mathcal{M}}^2 [\mathcal{C}(2)]^2}{3 \cdot 3 \cdot (2!)^2 \cdot 8 \cdot 8 \cdot 8^{J_2} \cdot 8^{J_2}} \leq CM_2^{-6} \leq \widehat{CM}^{-6}, \end{aligned} \quad (4.9)$$

370 where $\widehat{M} = \min\{M_1, M_2\}$. Proceeding in a similar way, one can obtain the following bounds:

$$\begin{cases} \mathcal{I}_2 \leq CM_1^{-6} \leq C\widehat{M}^{-6}, \\ \mathcal{I}_3 \leq CM_1^{-6}M_2^{-6} \leq C\widehat{M}^{-12} \leq C\widehat{M}^{-6}, \\ \mathcal{I}_4 \leq CM_1^{-3}M_2^{-3} \leq C\widehat{M}^{-6}, \\ \mathcal{I}_5 \leq CM_1^{-3}M_2^{-6} \leq C\widehat{M}^{-9} \leq C\widehat{M}^{-6}, \\ \mathcal{I}_6 \leq CM_1^{-6}M_2^{-3} \leq C\widehat{M}^{-9} \leq C\widehat{M}^{-6}. \end{cases} \quad (4.10)$$

Substituting (4.9)-(4.10) into (4.8), and then, taking the square root of both sides, one can obtain the desired error bound. \square

The following theorem demonstrates the error bounds for the solution of the semi-discretized form (3.16) of the proposed two-dimensional TFIPDEs, which helps to estimate the error bound in Theorem 4.10 of the
375 fully discretized numerical solution obtained by the $L2-1_\sigma$ scheme and Haar wavelet.

Theorem 4.9. *The solution of the semi-discretized problem (3.16) satisfies the following error bound.*

$$\left| \mathcal{U}(x, y, t_{n+1}) - \mathcal{U}^{n+1}(x, y) \right| \leq C[(\Delta t)^{3-\alpha} + (\Delta t)^2], \text{ for } n = 0, 1, \dots, N-1.$$

Proof. Keeping in mind the remainder term depicted in (3.17), based on the stability estimate given in Theorem 4.2, and proceeding in a similar way as described in Theorem 4.3, this theorem can be proved. \square

Now, we present the main convergence result that occurred from the fully discrete solution of the two-
380 dimensional TFIPDEs (1.2) based on $L2-1_\sigma$ scheme and the Haar wavelets.

Theorem 4.10. *The solution of the fully discrete form of the given two-dimensional TFIPDEs satisfies the following error bound.*

$$\left\| \mathcal{U}(x, y, t_{n+1}) - \mathcal{U}_{M_1 M_2}^{n+1}(x, y) \right\|_{L^2} \leq C[(\Delta t)^{3-\alpha} + (\Delta t)^2 + \widehat{M}^{-3}].$$

Proof. Applying triangle inequality, and using Theorems 4.8 & 4.9, we have

$$\begin{aligned} \left\| \mathcal{U}(x, y, t_{n+1}) - \mathcal{U}_{M_1 M_2}^{n+1}(x, y) \right\|_{L^2} &\leq \left\| \mathcal{U}(x, y, t_{n+1}) - \mathcal{U}^{n+1}(x, y) \right\|_{L^2} + \left\| \mathcal{U}^{n+1}(x, y) - \mathcal{U}_{M_1 M_2}^{n+1}(x, y) \right\|_{L^2} \\ &\leq \left\| \mathcal{U}(x, y, t_{n+1}) - \mathcal{U}^{n+1}(x, y) \right\|_{\infty} + \left\| \mathcal{U}^{n+1}(x, y) - \mathcal{U}_{M_1 M_2}^{n+1}(x, y) \right\|_{L^2} \\ &\leq C[(\Delta t)^{3-\alpha} + (\Delta t)^2 + \widehat{M}^{-3}]. \end{aligned}$$

\square

385 **Note 4.** *It can be noticed that the combination of the $L2-1_\sigma$ scheme and the Haar wavelet approximation for the two-dimensional TFIPDEs yields the higher-order approximation in time-space i.e. second-order as expected, which is also shown experimentally in Section 5 (see Figure 9 and Tables 6, 7 & 8).*

5. Results and discussion

In this section, we consider numerous examples of one and two-dimensional TFIPDEs to demonstrate the effectiveness and high accuracy of the proposed method. The results are compared with the results obtained by $L1$ scheme. Several tests are performed and the results are shown in the shape of figures and tables.

Example 5.1. Consider the following TFIPDE of the form:

$$\begin{cases} \partial_t^\alpha \mathcal{U}(x, t) - (1+x)\mathcal{U}_{xx} + \mathcal{U}(x, t) + \int_0^t \mathcal{K}(x, t-\xi)\mathcal{U}(x, \xi)d\xi = f(x, t), & (x, t) \in [0, 1] \times (0, 1], \\ \text{with initial and boundary conditions:} \\ \mathcal{U}(x, 0) = \sin \pi x \quad \forall x \in [0, 1], \quad \mathcal{U}(0, t) = 0, \quad \mathcal{U}(1, t) = 0 \quad \forall t \in (0, 1], \end{cases}$$

where $\alpha \in (0, 1)$. The kernel $\mathcal{K}(x, t-\xi) = (t-\xi) \sin x$ and $f(x, t)$ is given by:

$$\begin{aligned} f(x, t) = & \frac{\Gamma(\alpha+5)}{24} t^4 \sin \pi x + \pi^2 (1+t^{\alpha+4})(1+x) \sin \pi x + (1+t^{\alpha+4}) \sin \pi x \\ & + \left(\frac{t^2}{2} + \frac{t^{\alpha+6}}{(\alpha+5)(\alpha+6)} \right) \sin x \sin \pi x. \end{aligned}$$

The exact solution for Example 5.1 is $\mathcal{U}(x, t) = (1+t^{\alpha+4}) \sin \pi x$. If $\{\mathcal{U}(x_m, t_n)\}_{m=0, n=0}^{M, N}$ denotes the exact solution and $\{\mathcal{U}_m^n\}_{m=0, n=0}^{M, N}$ is the numerical solution of Example 5.1 by using the proposed scheme (3.8), then the computed error $\hat{E}_{M, N}$ and the corresponding rate of convergence $\hat{P}_{M, N}$ are estimated as:

$$\hat{E}_{M, N} = \max_{(x_m, t_n) \in \Omega_{M, N}} |\mathcal{U}(x_m, t_n) - \mathcal{U}_m^n|, \quad \hat{P}_{M, N} = \log_2 \left(\frac{\hat{E}_{M, N}}{\hat{E}_{2M, 2N}} \right). \quad (5.1)$$

The graphical representation of the exact and the corresponding numerical solution is portrayed in Figure 1(a) and Figure 1(b), respectively with $\alpha = 0.3$ for $M = 32, N = 64$. The surface displayed in Figure 2(a) depicts the maximum error for different values of α for $M = N$. From this representation, it is observed that the error plot decreases as N increases. This proves the convergence of the proposed method as proved theoretically in Theorem 4.3. The comparison of the results obtained by the proposed scheme with the results obtained by the $L1$ scheme is shown through a log-log plot in Figure 2(b) with $\alpha = 0.7$ for Example 5.1. It can be seen that the straight lines corresponding to the errors and the error bounds are in a parallel position by making an angle with the negative x-axis which is larger than the angle made by the $L1$ scheme. This proves that the $L2-1_\sigma$ scheme provides better accuracy than the $L1$ scheme in solving such TFIPDEs. The computed error ($\hat{E}_{M, N}$) and the order of convergence ($\hat{P}_{M, N}$) are displayed in tabular form in Table 1 for $\alpha = 0.2, 0.5, 0.8$, respectively. The data confirms the second-order convergence of the proposed scheme which satisfies our theoretical analysis proved in Theorem 4.3. The results depicted in Table 2 display the comparison between $L2-1_\sigma$ and $L1$ schemes with $\alpha = 0.1, 0.9$ for Example 5.1. From this illustration, it is clear that the proposed scheme gives second-order accuracy for any value of α whereas, $L1$ scheme exhibits almost first-order accuracy for α tends to 1 (see Remark 4.6).

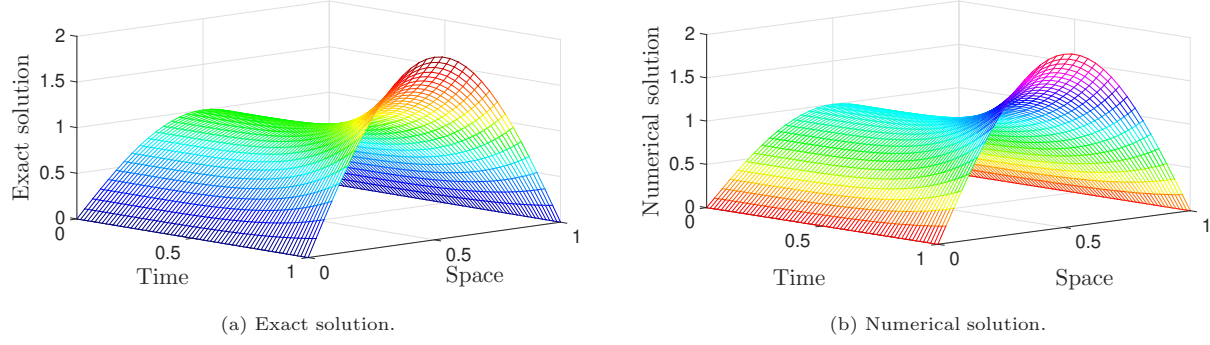


Figure 1: Solutions with $\alpha = 0.3$ and $M = 32, N = 64$ for Example 5.1.

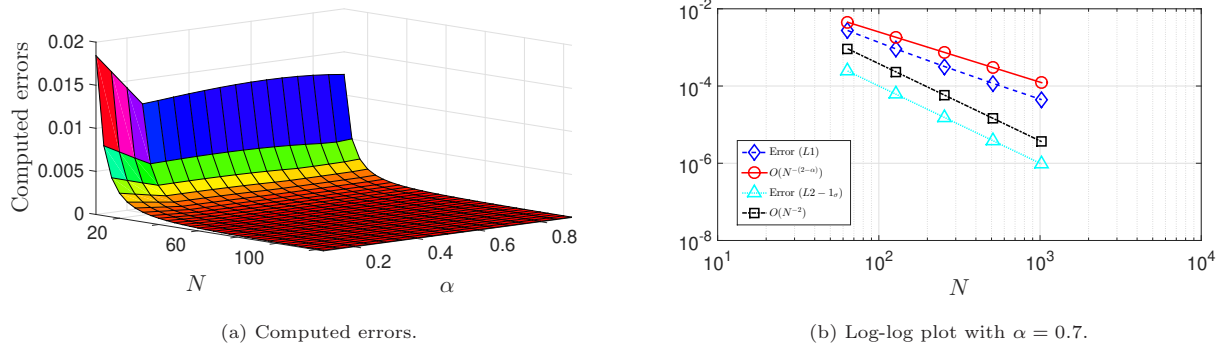


Figure 2: Error and log-log plots for Example 5.1.

Example 5.2. Let $\alpha \in (0, 1)$. Consider the following test problem:

$$\begin{cases} \partial_t^\alpha \mathcal{U}(x, t) - \mathcal{U}_{xx} + \int_0^t x(t - \xi) \mathcal{U}(x, \xi) d\xi = f(x, t), & (x, t) \in [0, 1] \times (0, 1], \\ \text{with initial and boundary conditions:} \\ \mathcal{U}(x, 0) = 0 \quad \forall x \in [0, 1], \quad \mathcal{U}(0, t) = t + t^{\alpha+3}, \quad \mathcal{U}(1, t) = 0 \quad \forall t \in (0, 1], \end{cases}$$

where $f(x, t)$ is given by: $f(x, t) = (1 - x^2) \left(\frac{t^{1-\alpha}}{\Gamma(2-\alpha)} + \frac{1}{6} \Gamma(\alpha+4) t^3 \right) + 2(t + t^{\alpha+3}) + x(1 - x^2) \left(\frac{t^3}{6} + \frac{t^{\alpha+5}}{(\alpha+4)(\alpha+5)} \right)$. The exact solution for Example 5.2 is $\mathcal{U}(x, t) = (1 - x^2)(t + t^{\alpha+3})$. The error and the rate of convergence are calculated by the same formula as defined in (5.1).

We display the surface plots of the exact solution and the respective numerical solution in Figure 3 with $\alpha = 0.5$ for $M = 32, N = 64$. The comparison results are shown in Figure 4(a) in terms of maximum error, and in Figure 4(b) based on log-log plot. It is clearly observed that the proposed scheme (3.8) not only gives higher order accuracy (see Figure 4(b)) but also the obtained errors are less (see Figure 4(a)) compared to the $L1$ scheme. The error and the convergence rate are also shown in Table 3 for $\alpha = 0.3, 0.6, 0.9$, respectively based on $L2-1_\sigma$ scheme as well as the $L1$ scheme, by fixing $M = N$. Further, we display the comparison results in Table 4 for $\alpha = 0.2, 0.5, 0.8$, respectively by taking unequal mesh sizes for Example

Table 1: $\hat{E}_{M,N}$ and $\hat{P}_{M,N}$ by $L2-1\sigma$ scheme for Example 5.1.

N/M	$\alpha = 0.2$		$\alpha = 0.5$		$\alpha = 0.8$	
	Maximum	Rate of	Maximum	Rate of	Maximum	Rate of
	errors	convergence	errors	convergence	errors	convergence
32/16	5.0469e-3	2.0028	4.2082e-3	2.0032	3.4737e-3	2.0010
64/32	1.2592e-3	2.0010	1.0497e-3	2.0009	8.6779e-4	1.9990
128/64	3.1459e-4	2.0004	2.6226e-4	2.0001	2.1710e-4	1.9984
256/128	7.8628e-5	2.0001	6.5560e-5	1.9998	5.4334e-5	1.9982
512/256	1.9655e-5		1.6392e-5		1.3601e-5	

5.2. In conclusion with the numerical results depicted in Tables 3 and 4, it is clear that the proposed method provides better accuracy namely second-order (see also Note 2) for any value of α , but on the contrary, the $L1$ scheme gives $2 - \alpha$ rate of convergence (see Note 3) for $\alpha \in (0, 1)$, and exhibits a first order convergence rate as α tends to one (see also Remark 4.6).

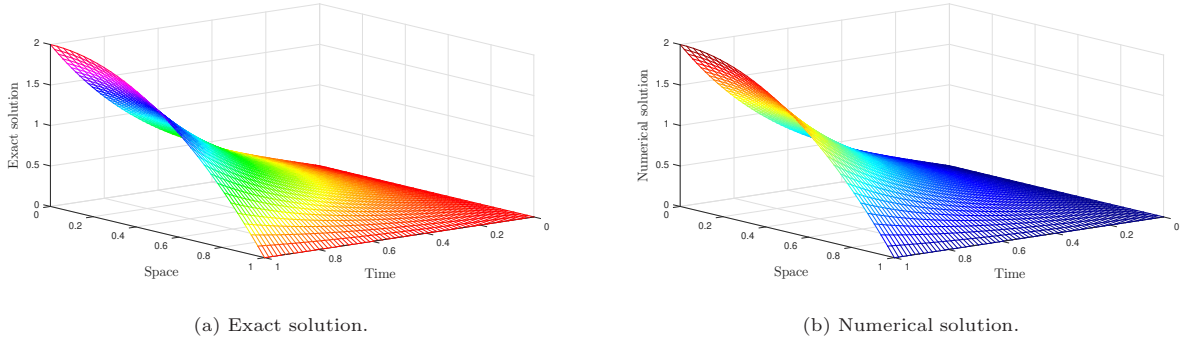


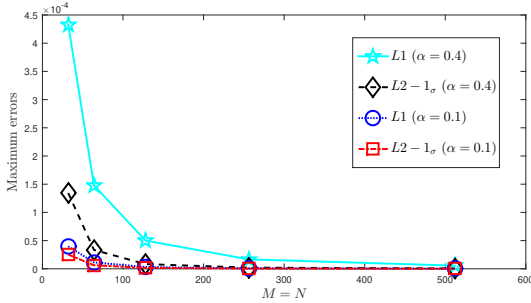
Figure 3: Solutions with $\alpha = 0.5$ and $M = 32, N = 64$ for Example 5.2.

Below, we present another example of the type (1.1) for which the exact solution is unknown. The double mesh principle [28] is used to calculate the error and the order of convergence as follows: Suppose \mathcal{U}_m^n be the numerical solution for $m = 0, 1, \dots, M$ and $n = 0, 1, \dots, N$. Now consider a fine mesh $\{(x_{m/2}, t_{n/2}) \mid m = 0, 1, \dots, 2M \text{ and } n = 0, 1, \dots, 2N\}$, and let $\mathcal{V}_{m/2}^{n/2}$ be the corresponding computed solution by using the same scheme. Then the error and the corresponding convergence rate are estimated as:

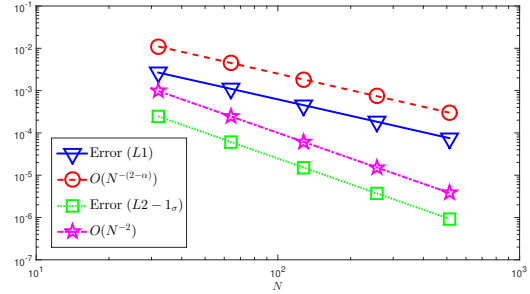
$$\tilde{E}_{M,N} := \max_{(x_m, t_n) \in \Omega_{M,N}} |\mathcal{U}_m^n - \mathcal{V}_m^n|, \quad \tilde{P}_{M,N} := \log_2 \left(\frac{\tilde{E}_{M,N}}{\tilde{E}_{2M,2N}} \right). \quad (5.2)$$

Table 2: Comparison of $\hat{E}_{M,N}$ and $\hat{P}_{M,N}$ between $L1$ and $L2-1_\sigma$ schemes for Example 5.1.

α	N/M	$L2-1_\sigma$ scheme		$L1$ scheme	
		Maximum errors	Rate of convergence	Maximum errors	Rate of convergence
0.1	64/32	1.3317e-3	2.0008	1.4125e-3	1.9983
	128/64	3.3275e-4	2.0003	3.5353e-4	1.9978
	256/128	8.3170e-5	2.0001	8.8517e-5	1.9976
	512/256	2.0791e-5	2.0000	2.2167e-5	1.9973
	1024/512	5.1977e-6		5.5519e-6	
0.9	64/32	8.1502e-4	1.9988	5.9369e-3	1.2465
	128/64	2.0393e-4	1.9982	2.5022e-3	1.1855
	256/128	5.1046e-5	1.9980	1.1002e-3	1.1479
	512/256	1.2779e-5	1.9981	4.9648e-4	1.1263
	1024/512	3.1991e-6		2.2743e-4	



(a) Maximum errors.



(b) Log-log plot with $\alpha = 0.7$.

Figure 4: Comparison between $L1$ and $L2-1_\sigma$ schemes for Example 5.2.

Example 5.3. Consider another TFIPDE of the form:

$$\begin{cases} \partial_t^\alpha \mathcal{U}(x, t) - \mathcal{U}_{xx} + x\mathcal{U}(x, t) + \int_0^t \mathcal{K}(x, t - \xi)\mathcal{U}(x, \xi)d\xi = xt^{4+\alpha}, & (x, t) \in [0, 1] \times (0, 1], \\ \text{with initial and boundary conditions:} \\ \mathcal{U}(x, 0) = 0 \quad \forall x \in [0, 1], \quad \mathcal{U}(0, t) = \mathcal{U}(1, t) = 0 \quad \forall t \in (0, 1], \end{cases}$$

where $\alpha \in (0, 1)$, and the kernel $\mathcal{K} = e^{x(t-\xi)}$, $\xi \in [0, t]$, $t \in [0, 1]$. We solve the model by using the proposed scheme (3.8) and the results are displayed in the shape of figures and tables. The graphical representation of the numerical solution is displayed in Figure 5 through contour plot (see Figure 5(a)) and surface plot (see Figure 5(b)), respectively. Since the exact solution is unknown, we calculate the error and the rate of convergence by using the formula depicted in (5.2), and the data are tabulated in Table 5 for $\alpha = 0.3, 0.6, 0.9$. It can also be observed that the obtained rate of convergence is almost second-order in

Table 3: Comparison of $\hat{E}_{M,N}$ and $\hat{P}_{M,N}$ between $L1$ and $L2-1_\sigma$ schemes for Example 5.2.

α	$N = M$	$L2-1_\sigma$ scheme		$L1$ scheme	
		Maximum	Rate of	Maximum	Rate of
		errors	convergence	errors	convergence
0.3	32	9.7316e-5	2.0034	2.1852e-4	1.6371
	64	2.4271e-5	2.0036	7.0256e-5	1.6515
	128	6.0525e-6	2.0029	2.2363e-5	1.6623
	256	1.5100e-6	2.0022	7.0654e-6	1.6703
	512	3.7692e-7		2.2199e-6	
0.6	32	2.0888e-4	2.0125	1.4945e-3	1.3694
	64	5.1770e-5	2.0117	5.7843e-4	1.3809
	128	1.2838e-5	2.0100	2.2211e-4	1.3879
	256	3.1874e-6	2.0082	8.4874e-5	1.3922
	512	7.9234e-7		3.2335e-5	
0.9	32	3.2295e-4	2.0117	7.9829e-3	1.0835
	64	8.0085e-5	2.0125	3.7669e-3	1.0914
	128	1.9848e-5	2.0125	1.7679e-3	1.0955
	256	4.9192e-6	2.0121	8.2735e-4	1.0976
	512	1.2196e-6		3.8661e-4	

the context of TFIPDEs, which confirms the theoretical analysis described in Theorem 4.3.

440

The following example shows the strong reliability of the wavelet-based numerical approximation combined with $L2-1_\sigma$ scheme described in Section 3.2 in the context of two-dimensional TFIPDEs of type (1.2). The maximum absolute error $\mathcal{E}_N^{M_1 M_2}$ (L^∞ -error) and the L^2 -error $\tilde{\mathcal{E}}_N^{M_1 M_2}$ can be estimated as:

$$\begin{cases} \mathcal{E}_N^{M_1 M_2} = \max_{1 \leq n \leq N} \max_{1 \leq l_1 \leq 2M_1} \max_{1 \leq l_2 \leq 2M_2} |\mathcal{U}(x_{l_1}, y_{l_2}, t_n) - \mathcal{U}_{M_1 M_2}^n(x_{l_1}, y_{l_2})|, \\ \tilde{\mathcal{E}}_N^{M_1 M_2} = \left[\frac{1}{2M_1 \times 2M_2 \times N} \sum_{l_1=1}^{2M_1} \sum_{l_2=1}^{2M_2} \sum_{n=1}^N |\mathcal{U}(x_{l_1}, y_{l_2}, t_n) - \mathcal{U}_{M_1 M_2}^n(x_{l_1}, y_{l_2})|^2 \right]^{1/2}. \end{cases} \quad (5.3)$$

The corresponding temporal rate of convergence can be calculated by the usual way as:

$$\mathcal{R}_N^{M_1 M_2} = \log_2 \left(\frac{\mathcal{E}_N^{M_1 M_2}}{\mathcal{E}_{2N}^{M_1 M_2}} \right), \quad \tilde{\mathcal{R}}_N^{M_1 M_2} = \log_2 \left(\frac{\tilde{\mathcal{E}}_N^{M_1 M_2}}{\tilde{\mathcal{E}}_{2N}^{M_1 M_2}} \right). \quad (5.4)$$

Table 4: Comparison of $\hat{E}_{M,N}$ and $\hat{P}_{M,N}$ between $L1$ and $L2-1_\sigma$ schemes for Example 5.2.

α	N/M	$L2-1_\sigma$ scheme		$L1$ scheme	
		Maximum errors	Rate of convergence	Maximum errors	Rate of convergence
0.2	32/16	6.0734e-5	2.0006	1.0166e-4	1.7225
	64/32	1.5177e-5	2.0018	3.0805e-5	1.7361
	128/64	3.7896e-6	2.0016	9.2471e-6	1.7466
	256/128	9.4633e-7	2.0012	2.7556e-6	1.7555
	512/256	2.3638e-7		8.1611e-7	
0.5	32/16	1.7163e-4	2.0088	8.1809e-4	1.4617
	64/32	4.2647e-5	2.0085	2.9702e-4	1.4741
	128/64	1.0599e-5	2.0071	1.0691e-4	1.4824
	256/128	2.6368e-6	2.0055	3.8263e-5	1.4878
	512/256	6.5667e-7		1.3643e-5	
0.8	32/16	2.8351e-4	2.0154	4.6544e-3	1.1803
	64/32	7.0123e-5	2.0157	2.0539e-3	1.1890
	128/64	1.7341e-5	2.0146	9.0084e-4	1.1939
	256/128	4.2917e-6	2.0135	3.9378e-4	1.1966
	512/256	1.0629e-6		1.7181e-4	

Example 5.4. Examine the following two-dimensional TFIPDE:

$$\left\{ \begin{array}{l} \partial_t^\alpha \mathcal{U}(x, y, t) - \mathcal{U}_{xx} - \mathcal{U}_{yy} + \mathcal{U}_x + \int_0^t xy(t - \xi) \mathcal{U}(x, y, \xi) d\xi = f(x, y, t), \quad (x, y, t) \in \mathcal{G} \times (0, 1], \\ \text{with initial and boundary conditions:} \\ \mathcal{U}(x, y, 0) = xy(x - 1)(y - 1) \quad \forall (x, y) \in \mathcal{G}, \\ \mathcal{U}(0, y, t) = \mathcal{U}(1, y, t) = 0 \quad \forall (y, t) \in [0, 1] \times (0, 1], \\ \mathcal{U}(x, 0, t) = \mathcal{U}(x, 1, t) = 0 \quad \forall (x, t) \in [0, 1] \times (0, 1], \end{array} \right.$$

where $\alpha \in (0, 1)$. The source function f is given by:

$$\begin{aligned} f(x, y, t) = & \frac{1}{6} \Gamma(\alpha + 4) xy(x - 1)(y - 1) t^3 - 2(1 + t^{\alpha+3})(x^2 + y^2 - x - y) \\ & + (1 + t^{\alpha+3})(2x - 1)(y^2 - y) + \left(\frac{t^2}{2} + \frac{t^{\alpha+5}}{(\alpha + 4)(\alpha + 5)} \right) x^2 y^2 (x - 1)(y - 1). \end{aligned}$$

The exact solution for Example 5.4 is $\mathcal{U} = (1 + t^{\alpha+3})xy(x - 1)(y - 1)$. To solve the model, the $L2-1_\sigma$ scheme is used to make it in a semi-discretization form as described in (3.16). Then, at each time level, the two-dimensional Haar wavelet is applied to approximate the solution.

The surfaces displayed in Figures 6(a) and 6(b) demonstrate the exact and the computed solution for Example 5.4 with $\alpha = 0.6$, $2M_1 = 2M_2 = 64$ at $t = 1$ by discretizing the temporal direction with a

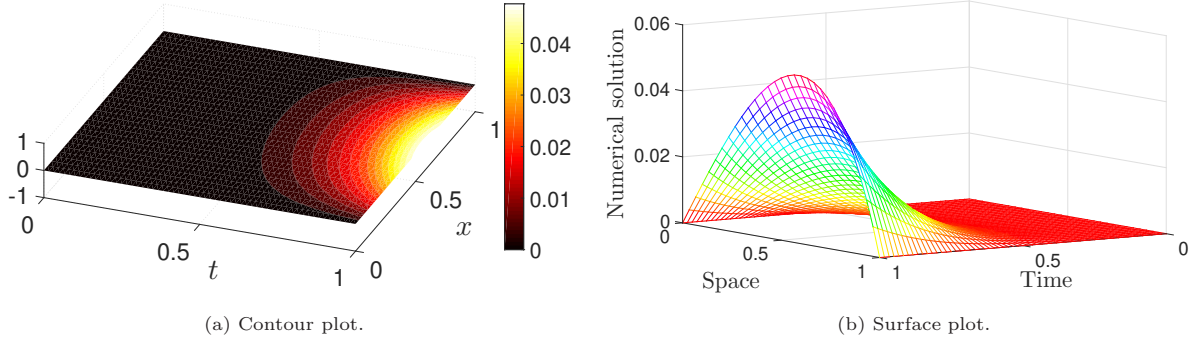
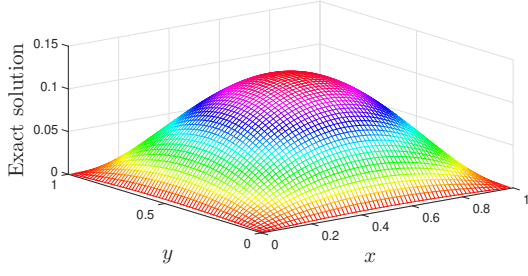


Figure 5: Graphical representation with $\alpha = 0.4$, $M = 30$, $N = 60$ for Example 5.3.

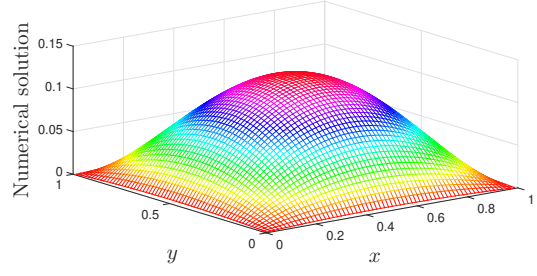
Table 5: $\tilde{E}_{M,N}$ and $\tilde{P}_{M,N}$ by $L2-1_\sigma$ scheme for Example 5.3.

N/M	$\alpha = 0.3$		$\alpha = 0.6$		$\alpha = 0.9$	
	Maximum errors	Rate of convergence	Maximum errors	Rate of convergence	Maximum errors	Rate of convergence
16/32	1.2692e-4	1.9786	2.2421e-4	1.9872	2.8086e-4	1.9954
32/64	3.2205e-5	1.9907	5.6552e-5	1.9971	7.0437e-5	2.0018
64/128	8.1033e-6	1.9962	1.4166e-5	2.0009	1.7587e-5	2.0037
128/256	2.0312e-6	1.9986	3.5393e-6	2.0023	4.3856e-6	2.0045
256/512	5.0828e-7		8.8345e-7		1.0930e-6	

step length $\Delta t = 1/10$. The contour plot representation of the exact and numerical solution is shown in Figure 7 for $\alpha = 0.4$, $2M_1 = 2M_2 = 32$ at $t = 0.5$ with $\Delta t = 1/10$. The cross-sectional view with fixed $x = y = 9.6875e - 1$ and varying t is shown in Figure 8(a), which essentially illustrates the comparison between the exact and numerical solution in the context of a two-dimensional TFIPDE. One can see that the numerical solution is very close to the exact solution. In contrast, Figure 8(b) demonstrates the absolute point-wise error at $t = 1$. Here, we have chosen $2M_1 = 2M_2 = 16$, $\alpha = 0.7$ and $\Delta t = 1/20$. We calculate the error and the order convergence by using the formula given in (5.3) and (5.4). The numerical data is exactly matched with our theoretical estimate proved in Theorem 4.10 (see also Note 4), which illustrates that the proposed scheme based on the Haar wavelets and $L2-1_\sigma$ scheme produces a higher-order accuracy (possibly second-order) for any values of $\alpha \in (0, 1)$ (for example, see Tables 6, 7, & 8, which display the computed error and the corresponding rate of convergence based on L^2 and L^∞ norm for different values of $\alpha = 0.2, 0.4, 0.8$, respectively). The high accuracy convergence rate can also be confirmed from Figure 9, which shows the log-log plot with $2M_1 = 2M_2 = 32$, $\alpha = 0.3$ for Example 5.4.

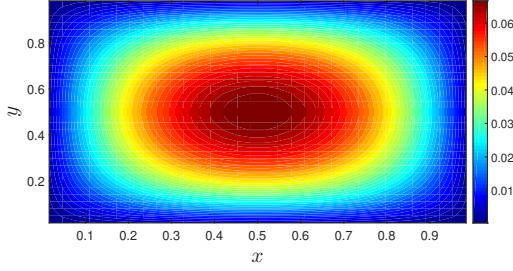


(a) Exact solution.

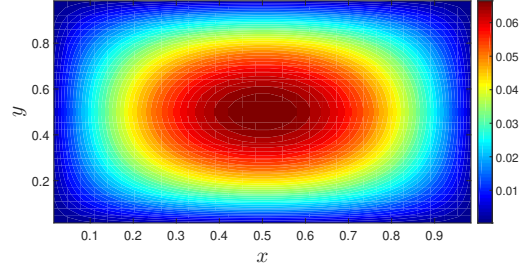


(b) Numerical solution.

Figure 6: Surface plots with $\alpha = 0.6$ and $2M_1 = 2M_2 = 64$ at $t = 1$ with $\Delta t = 1/10$ for Example 5.4.

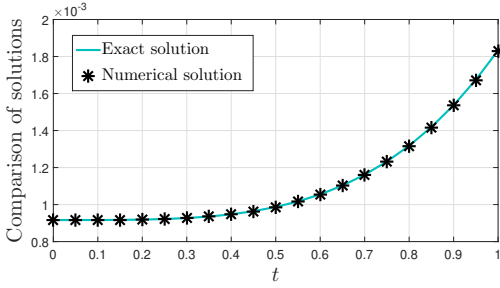


(a) Exact solution.

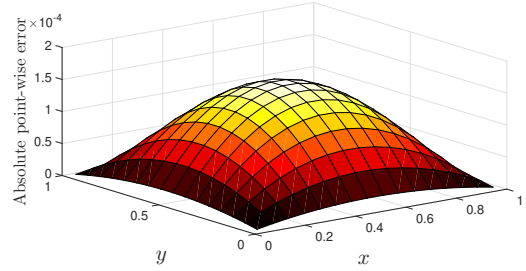


(b) Numerical solution.

Figure 7: Contour plot representation with $\alpha = 0.4$ and $2M_1 = 2M_2 = 32$ at $t = 0.5$ with $\Delta t = 1/10$ for Example 5.4.

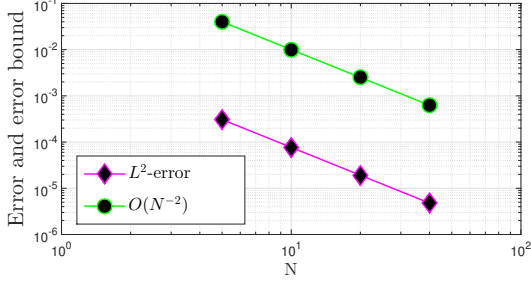


(a) $x = y = 9.6875e - 1$.

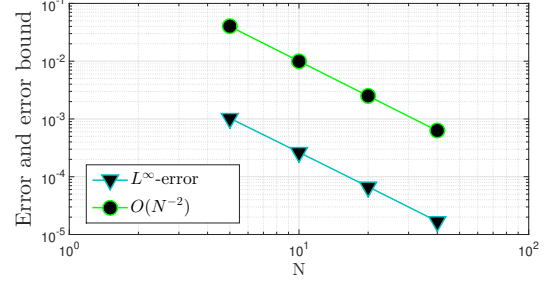


(b) Absolute point-wise error at $t = 1$.

Figure 8: Graphical representation with $2M_1 = 2M_2 = 16$, $\alpha = 0.7$ and $\Delta t = 1/20$ for Example 5.4.



(a) L^2 -error.



(b) L^∞ -error.

Figure 9: Log-log plots with $2M_1 = 2M_2 = 32$, $\alpha = 0.3$ for Example 5.4.

Table 6: Example 5.4, with $2M_1 = 2M_2 = 16$ for $\alpha = 0.2$.

Δt	L^2 -error	Order	L^∞ -error	Order
1/5	2.0560e-4	1.990	6.7234e-4	1.956
1/10	5.1746e-5	1.997	1.7324e-4	1.980
1/20	1.2966e-5	1.999	4.3917e-5	1.991
1/40	3.2433e-6		1.1050e-5	

Table 7: Example 5.4, with $2M_1 = 2M_2 = 32$ for $\alpha = 0.4$.

Δt	L^2 -error	Order	L^∞ -error	Order
1/5	4.0744e-4	2.012	1.3910e-3	1.962
1/10	1.0101e-4	2.010	3.5696e-4	1.984
1/20	2.5082e-5	2.007	9.0253e-5	1.993
1/40	6.2403e-6		2.2668e-5	

6. Concluding remarks

465 This paper presents a numerical approximation based on the $L2-1_\sigma$ scheme for solving a class of time-fractional integro-PDEs with Caputo fractional derivatives. The approach is extended to two-dimensional fractional integro-PDEs, with wavelet-based numerical approximation used to approximate the spatial derivatives at each time level. The stability and convergence of the method are demonstrated both theoretically and computationally. To demonstrate the reliability of the proposed method, the results are compared to
 470 those of the $L1$ scheme. It is shown that the proposed method not only provides higher-order accuracy for

Table 8: Example 5.4, with $2M_1 = 2M_2 = 32$ for $\alpha = 0.8$.

Δt	L^2 -error	Order	L^∞ -error	Order
1/5	7.5992e-4	2.060	2.7544e-3	1.980
1/10	1.8226e-4	2.038	6.9799e-4	1.995
1/20	4.4364e-5	2.024	1.7513e-4	2.000
1/40	1.0910e-5		4.3772e-5	

solving the given models but also produces less error than the $L1$ scheme in favor of one and two-dimensional TFIPDEs. The computational results support the theoretical arguments.

Declarations

Acknowledgement

475 Sudarshan Santra wants to acknowledge the Axis Bank Centre for Mathematics and Computing, Indian Institute of Science, Bangalore for the financial assistance to carry out this research work in the Department of Computational and Data Sciences, Indian Institute of Science, Bangalore.

Ethical Approval

480 The authors follow the basic ethics of the present journal. The present work is neither published nor under consideration at other places.

Funding Details

Ratikanta Behera is grateful for the support from the Science and Engineering Research Board (SERB), Department of Science and Technology, India, under Grant No. SRG/2023/002710.

Data Availability Statements

485 The data sets generated during and/or analyzed during the current study are available from the corresponding author upon reasonable request.

Conflicts of Interest

The authors declare that there are no conflicts of interest.

Informed Consent

490 On behalf of the authors, Dr. Ratikanta Behera shall be communicating the manuscript.

Authors Information

Sudarshan Santra^a, Ratikanta Behera^a

Affiliations:

^aDepartment of Computational and Data Sciences, Indian Institute of Science, Bangalore, India

Corresponding author:

Correspondence to Ratikanta Behera.

Consent for Publication

All authors provide their consent for publication.

Human and Animal Ethics

Not Applicable.

References

- [1] C. A. Monje, Y. Chen, B. M. Vinagre, D. Xue, V. Feliu, Müntz-legendre wavelet operational matrix of fractional-order integration and its applications for solving the fractional Pantograph differential equations, Fractional-order systems and controls, Advances in Industrial Control, Springer, London.
- [2] M. A. Ichou, H. E. Amri, A. Ezziani, On existence and uniqueness of solution for space-time fractional Zener model, Acta Appl. Math. 170 (2020) 593–609.
- [3] V. Mehandiratta, M. Mehra, G. Leugering, An approach based on Haar wavelet for the approximation of fractional calculus with application to initial and boundary value problems, Math. Methods Appl. Sci. 44 (4) (2021) 3195–3213.
- [4] H. Chen, F. Holland, M. Stynes, An analysis of the Grunwald-Letnikov scheme for initial-value problems with weakly singular solutions, Appl. Numer. Math. 139 (2019) 52–61.
- [5] S. Santra, J. Mohapatra, Analysis of a finite difference method based on L1 discretization for solving multi-term fractional differential equation involving weak singularity, Math. Methods Appl. Sci. 45 (11) (2022) 6677–6690.
- [6] J. Mohapatra, S. Santra, H. Ramos, Analytical and numerical solution for the time fractional black-scholes model under jump-diffusion, Comput. Econ. 68 (5) (2022) 3545–3563.
- [7] S. Abbasbandy, M. S. Hashemi, I. Hashim, On convergence of homotopy analysis method and its application to fractional integro-differential equations, Quaest. Math. 36 (1) (2013) 93–105. doi:10.2989/16073606.2013.780336.

- 520 [8] A. A. Hamoud, K. P. Ghadle, Modified Laplace decomposition method for fractional Volterra-Fredholm integro-differential equations, *J. Math. Model.* 6 (1) (2018) 91–104.
- [9] A. Babaei, S. Banihashemi, C. Cattani, An efficient numerical approach to solve a class of variable-order fractional integro-partial differential equations, *Numer. Methods Partial Differential Equations* 37 (1) (2021) 674–689. doi:10.1002/num.22546.
- 525 [10] M. Dehghan, M. Abbaszadeh, A Legendre spectral element method (SEM) based on the modified bases for solving neutral delay distributed-order fractional damped diffusion-wave equation, *Math. Methods Appl. Sci.* 41 (9) (2018) 3476–3494.
- [11] L. Brugnano, G. Frasca-Caccia, F. Iavernaro, V. Vespri, A new framework for polynomial approximation to differential equations, *Adv. Comput. Math.* 48 (6). doi:10.1007/s10444-022-09992-w.
- 530 [12] L. Brugnano, F. Iavernaro, A general framework for solving differential equations, *Ann. Univ. Ferrara Sez. VII Sci. Mat.* 68 (2) (2022) 243–258.
- [13] R. Behera, M. Mehra, N. K.-R. Kevlahan, Multilevel approximation of the gradient operator on an adaptive spherical geodesic grid, *Adv. Comput. Math.* 41 (3) (2015) 663–689.
- [14] K. Schneider, O. V. Vasilyev, Wavelet methods in computational fluid dynamics, *Annu. Rev. Fluid Mech.*, Annual Reviews, Palo Alto, CA 42. doi:10.1146/annurev-fluid-121108-145637.
- 535 [15] N. Pervaiz, I. Aziz, Haar wavelet approximation for the solution of cubic nonlinear Schrodinger equations, *Phys. A* 545. doi:10.1016/j.physa.2019.123738.
- [16] S. ul Islam, I. Aziz, F. Haq, A comparative study of numerical integration based on Haar wavelets and hybrid functions, *Comput. Math. Appl.* 59 (6) (2010) 2026–2036.
- 540 [17] K. S. Miller, B. Ross, An introduction to the fractional calculus and fractional differential equations, John Wiley & Sons, Inc., New York, 1993.
- [18] Y. Han, X. Huang, W. Gu, B. Zheng, Linearized transformed $L1$ finite element methods for semi-linear time-fractional parabolic problems, *Appl. Math. Comput.* 458 (2023) Paper No. 128242, 14. doi:10.1016/j.amc.2023.128242.
- 545 [19] J. L. Gracia, E. O’Riordan, M. Stynes, Convergence in positive time for a finite difference method applied to a fractional convection-diffusion problem, *Comput. Methods Appl. Math.* 18 (1) (2018) 33–42.
- [20] G. h. Gao, Z. z. Sun, Y. n. Zhang, A finite difference scheme for fractional sub-diffusion equations on an unbounded domain using artificial boundary conditions, *J. Comput. Phys.* 231 (7) (2012) 2865–2879.

- [21] M. Li, Y. Wei, B. Niu, Y.-L. Zhao, Fast L_2 - 1_σ Galerkin FEMs for generalized nonlinear coupled Schrodinger equations with Caputo derivatives, Appl. Math. Comput. 416 (2022) Paper No. 126734, 22. doi:10.1016/j.amc.2021.126734.
- [22] A. A. Alikhanov, C. Huang, A high-order L_2 type difference scheme for the time-fractional diffusion equation, Appl. Math. Comput. 411 (2021) Paper No. 126545, 19. doi:10.1016/j.amc.2021.126545.
- [23] B. Guo, X. Pu, F. Huang, Fractional partial differential equations and their numerical solutions, World Scientific Publishing Co. Pte. Ltd., Hackensack, NJ, 2015.
- [24] H. G. Sun, W. Chen, Y. Q. Chen, Variable-order fractional differential operators in anomalous diffusion modeling, Physica A: Statistical Mechanics and its Applications 388 (21) (2009) 4586–4592.
- [25] R. Metzler, J. Klafter, The random walk’s guide to anomalous diffusion: a fractional dynamics approach, Appl. Numer. Math. 339 (1). doi:10.1016/S0370-1573(00)00070-3.
- [26] S. Konjik, L. Oparnica, D. Zorica, Waves in fractional Zener type viscoelastic media, J. Math. Anal. Appl. 365 (1) (2010) 259–268.
- [27] S. Santra, J. Mohapatra, A novel finite difference technique with error estimate for time fractional partial integro-differential equation of Volterra type, J. Comput. Appl. Math. 400. doi:10.1016/j.cam.2021.113746.
- [28] S. Santra, J. Mohapatra, Analysis of the L_1 scheme for a time fractional parabolic-elliptic problem involving weak singularity, Math. Methods Appl. Sci. 44 (2) (2021) 1529–1541.
- [29] S. Santra, A. Panda, J. Mohapatra, A novel approach for solving multi-term time fractional Volterra-Fredholm partial integro-differential equations, J. Appl. Math. Comput. doi:10.1007/s10614-023-10386-3.
- [30] G. h. Gao, Z. z. Sun, H. w. Zhang, A new fractional numerical differentiation formula to approximate the Caputo fractional derivative and its applications, J. Comput. Phys. 259 (2014) 33–50. doi:10.1016/j.jcp.2013.11.017.
- [31] A. A. Alikhanov, A new difference scheme for the time fractional diffusion equation, J. Comput. Phys. 280 (2015) 424–438. doi:10.1016/j.jcp.2014.09.031.
- [32] M. Stynes, Too much regularity may force too much uniqueness, Fract. Calc. Appl. Anal. 19 (6) (2016) 1554–1562. doi:10.1515/fca-2016-0080.
- [33] E. Kreyszig, Introductory functional analysis with applications, John Wiley & Sons, 1991.
- [34] W. Rudin, Principles of mathematical analysis, McGraw-hill, New York, 1976.

[35] J. Schauder, The fixed point theorem in functional spaces, *Studia Math.* 2 (1) (1930) 171–180.

580 [36] A. Haar, Zur Theorie der orthogonalen Funktionensysteme, *Math. Ann.* 69 (3) (1910) 331–371.

[37] S. ul Islam, I. A. B. Šarler, The numerical solution of second-order boundary-value problems by collocation method with the Haar wavelets, *Math. Comput. Modelling* 52 (9–10) (2010) 1577–1590.

[38] N. Wichailukkana, B. Novaprateep, C. Boonyasiriwat, A convergence analysis of the numerical solution of boundary-value problems by using two-dimensional haar wavelets, *Sci. Asia* 42 (2016) 346–355.
585 doi:10.2306/scienceasia1513-1874.2016.42.346.

[39] Y. Lin, C. Xu, Finite difference/spectral approximations for the time fractional diffusion equation, *J. Comput. Phys.* 225 (2) (2007) 1533–1552.

[40] Z. z. Sun, X. Wu, A fully discrete difference scheme for a diffusion-wave system, *Appl. Numer. Math.* 56 (2) (2006) 193–209.